POLITECNICO DI TORINO

Master of Science in Mechatronics Engineering

Master Thesis

Wind Farm Sliding Mode Control and Energy Optimization with Fatigue Contraints

Supervisors:
Dr. Elisa Capello

Prof. Yasumasa Fujisaki

Co-advisor:
Prof. Takayuki Wada

Candidate:
Andrea Cacciolatto

April, 2019

Abstract

Wind energy is the fastest growing market in the energy production, and it is estimated that by 2030, over the 20% of global energy production will be done with this technology. However, with the increase of dimensions of both the single turbines and of the clusters of wind turbines, generally known as wind farms, the engineering challenges increase too.

For defining the aerodynamic interaction between the four turbines, instead of assuming a linear deficit coefficient like in other researches, and considering that it is assumed that the turbines are installed in a diamond shape layout, a wake model, based on the Jensen model has been developed. This model shows how the overlapping effect between a wake and another turbine, reduces the wind input speed, reducing the available power to extract.

In this thesis, a model for a wind farm composed of four wind turbines and the relative control algorithms are presented. A simplified model for an Horizontal Axis Wind Turbine (HAWT) has been developed considering both the aerodynamics and the electrical generator. This last one has been developed considering a Doubly-Fed Induction Machine (DFIM) controlled and connected to the grid by a back-to-back converter, composed of two bi-directional voltage source inverters (VSI), where the stator windings of the generator are directly linked to the grid and the rotor windings are connected to the grid through the power converter. This configuration is the most used in industrial applications for its efficiency, reduced costs and reliability.

In order to control the single wind turbines, the standard approach implies the application of a vector control of the power converter where the control algorithm is generally based on the PI technique, which is simple to implement and tune but lacks of robustness and hardly deals with non linearities of plant model. In this thesis, a vector control based on the super-twisting sliding mode control (STW-SMC) for both the VSIs has been proposed. This control technique is characterized by a still simple control algorithm that guarantees robustness and low chattering effects. The results show a performance tracking of a desired rotational speed for the DFIMs, while the DC-bus voltage regulation for the grid side converter still presents too high ripples for considering it acceptable.

For the control of the entire wind farm system, the most common approach is the implementation of an algorithm for the maximum power extraction of the single turbines, but this approach doesn't take in consideration possible effects on the fatigue and damages imposed to the single wind turbine and on the potential wake interaction effects with the other turbines, which can cause an increase in the turbulence intensity and a consequent added mechanical stress on the other turbines of the system. Here, a supervisory control for the wind farm has been developed, based on an optimization algorithm that computes the best rotational speed

values for the single turbines, considering the wake interactions, in order to have a trade-off between power production, mechanical damages and turbulence generation. The results show how with this algorithm the wind farm power production is reduced but also the mechanical damages to the turbines are reduced, with the consequence of a possible increase in the lifetime of the system and of a reduction in the maintenance costs of the wind farm.

Sommario

L'energia eolica è il settore del mercato dell'energia più in rapida espansione, ed è stimato, che entro il 2030, oltre il 20% della produzione globale di energia verrà fatta con questa tecnologia. Tuttavia, con l'incremento delle dimensioni, sia delle singole turbine che degli assiemi di turbine eoliche, generalmente conosciute come parchi eolici, le sfide ingegneristiche aumentano.

Per definire l'interazione aerodinamica tra le quattro turbine, invece di assumere un coefficiente di riduzione di velocità di tipo lineare, e considerando che si assume una disposizione delle turbine di tipo a diamante, si è invece sviluppato un modello di scia basato sul modello di Jensen. Questo modello mostra come l'effetto di sovrapposizione tra la scia di una turbina ed un'altra turbina, riduce la velocità del vento in ingresso per quest'ultima, riducendo la potenza estraibile dal vento.

In questa tesi, un modello per una wind farm composta da quattro turbine e i relativi algoritmi e schemi di controllo sono presentati. Un modello semplificato per una turbina ad asse vertical (HAWT) è stato sviluppato considerando sia gli aspetti aerodinamici che il generatore elettrico. Quest'ultimo è stato sviluppando una macchina a doppio avvolgimento (DFIM) controllato e connesso alla rete attraverso un convertitore elettronico bi-direzionale, composto da due inverter a tensione impressa (VSI); in tale configurazione, gli avvolgimenti di statore sono collegati direttamente alla rete elettrica e quelli di avvolgimenti sono connessi alla rete tramite in convertitore. Questo tipo di configurazione è la più utilizzata in applicazioni industriali per la sua efficienza, i costi ridotti e l'affidabilità.

Per controllare le singole turbine eoliche, l'approcio standard implica l'applicazione di un controllo vettoriale dei convertitori di potenza dove l'algoritmo di controllo è generalmente basato sul tipo proporzionale-integrativo; tale algoritmo, che è di semplice implementazione, manca di proprietà di robustezza ed è poco efficace su modelli non-lineari del sistema. In questa tesi, un controllo vettoriale basato sul super-twisiting sliding mode control (STW-SMC) è stato implementato per entrambi i convertitori. Questo tipo di algoritmo, è sempre caratterizzato da una struttura semplice, ma che garantisce robustezza e bassi di livelli di chattering. I risultati ottenuti mostrano un buon inseguimento del valore di velocità desiderato per i DFIM, mentre la regolazione di tensione dell'accoppimento capacitivo dei convertitori di potenza presenta ancora ripple troppo alti per considerarsi accettabili.

Per il controllo dell'intero parco eolico, l'approcio più comune è l'implementazione di un algoritmo di tracciamento della massima potenza estraibile dalle singole turbine; tuttavia questo tipo di approcio non prendere in considerazione possibili effetti sui carichi strutturali, sui danni di fatica applicati sulle singole turbine e sulla potenziale interazione di scie con le altre turbine; queste ultime infatti, possono causare un incremento nell'intensità di turbolenza

ed un conseguente aumento di stress meccanico su altre turbine eoliche nel sistema. In questa tesi invece, si espone lo sviluppo di un diverso tipo di algoritmo di supervisione, che si basa su un algoritmo di ottimizzazione in grado di calcolare il miglior valore di velocità di rotazione per le singole turbine, considerando inoltre l'interazione aerodinamica; ciò permette di avere un compromesso tra potenza prodotta, danni alle turbine e turbolenza generata dalle scie. I risultati mostrano come, con questo algoritmo, la potenza estratta totale del parco eolico è ridotta, ma anche i carichi sulle turbine sono ridotti, con la conseguente possibilità di un incremento di vita dell'impinato e di una riduzione dei costi di manutenzione del parco eolico.

Acknowledgements

I would like to thank Dr. Elisa Capello for giving me the opportunity to work on a research field that will be fundamental for the next generations. Her support and tutoring has been fundamental for my work and personal growth as an engineer.

I would also like to thank Prof. Yasumasa Fujisaki and Prof. Takayuki Wada for their help and opportunity to go studying in their research lab in Osaka University. Their guidance had helped me understanding different points of view for solving a problem and how it is imperative to keep asking yourself how things can be done differently.

A special thank goes to the beautiful country of Japan, and specifically to the city of Osaka and its university, that given me the opportunity of living there for the period of my research. This has been an incredible opportunity for personal growth, enriched by the people that I've met.

A final thank goes to my family and friends, that supported me on this journey. Their help has been the fundamental factor for the last step of my academic studies, and for the realization of this thesis.

Contents

List of Figures

List of Tables

Chapter 1

INTRODUCTION

In this chapter, a short discussion of the nowadays's situation about the wind energy industry and research, followed by a brief introduction to the topic of this research and its main general assumptions is presented.

Figure 1.1: Gemini offshore wind farm, located in the Netherlands [2]

1.1 Research trends in wind energy

Since the beginning of the industrialization, the energy demands has globally increased, and the usage of fossil fuels, such as gas and oil, have brought considerable environmental damages. Fortunately, as well explained in [2], renewable energies such as wind and solar energy are on the rise, more precisely, it is estimated to grow to 33% of global power production by 2040.
Wind energy in particular is probably the fastest growing energy technology nowadays, where it is estimated, that just in the United States, by 2030, more than 20% of total energy will be produced by wind turbines [1]. The growth of the wind energy market has also brought an

increase of the engineering challenges to the proper application of this technology. As can be seen in Figure 1.2, the increase of the wind turbine is constantly increasing, and this brings challenges in terms of structures, manufacturing, installation, and of course design.

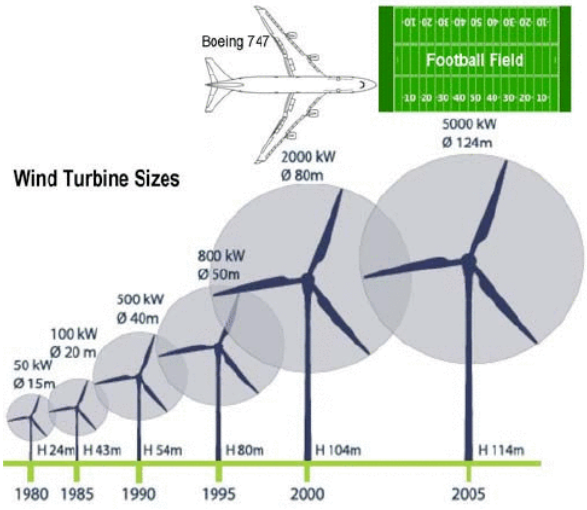

Figure 1.2: Comparison between dimensions of MW scale HAWT [1]

More in detail, one of the main challenges is given by the strategy of installing more wind turbines in a cluster, defined wind farm, in order to save space and to have an easier management of the energy plants. The closeness of this turbines brings problems related to wake interactions, that can cause power losses and mechanical stress, with the consequence of reducing the utility life of the turbines. So in order to design the wind energy conversion systems (WECS) it is necessary to also consider the need of the definition and application of mathematical models not only for the wind turbines themselves but also for their wakes, and how they interact with the other turbines, and what effects cause in the short and long term. Many researchers had worked on the development of this models, where a comprehensive review can be found in [28] and [7], where both linear and non-linear models are explained. Also, the need of a standard in the wind turbine modeling has been found in the NREL models of FAST, as can be read in [28], where the FAST model has been implemented for the aerodynamic model of a wind turbine equipped with a DFIG generator.

Figure 1.3: Wind farm in Galicia, Spain [1]

A major area of research, on which also this thesis has been focused on, is regarding the control algorithms, for both single turbines and clusters. The industrial approach regarding the single turbine control are based on the well known PI control, applied for both vector control and direct torque. Unfortunately, this kind of control law, doesn't possess properties that are fundamental in uncertain environments such as the WECS, first of all the robustness to un-modeled dynamics and measurement noise. The research has developed many alternatives, every-one with promising results but also drawbacks. In particular, sliding mode control techniques are one of the major interests at the moment. Various sliding mode control techniques have been tested, particular mention can go to [31] and [32] where sliding mode theory has been applied for both the control loops and for state observers. Other applications can be found found in [35], [36], [37] and [37]. Another interesting approach, is the application of the new trends of the neural networks to the sliding mode control, that can be found in [30]. Also other kinds of control techniques have been studied for wind turbine control, as can be seen in [34] with the application of a Linear Quadratic Gaussian, and in [33] with a tuned damping controller.

Regarding the supervisory control algorithm for the wind farm, in the standard approach the algorithms are based on the maximization of the power production of the single wind turbine, without regards for the entire cluster. This kind of control techniques are called Maximum Power Point Tracking (MPPT), and comprehensive reviews can be found in [42] and [43]. Another major trend, is about the development of better optimization and control algorithms for the obtaining the best results from the plant both in terms of energy production and degradation reduction, and various approach can be found in literature. For example, in [39], [40] and [41], a model predictive control approach has been implemented, while in [45] can be found an application of the binary particle swarm algorithm to the cas. Another interesting approach can be found in [44] with the application a genetic algorithm.

1.2 The goal of this research

The purpose of this research can be summarized in the following points:

1. The development of a mathematical model for an horizontal axis wind turbine, considering the conversion of the wind energy into mechanical energy

2. The development of a mathematical model for the wake interaction between turbines

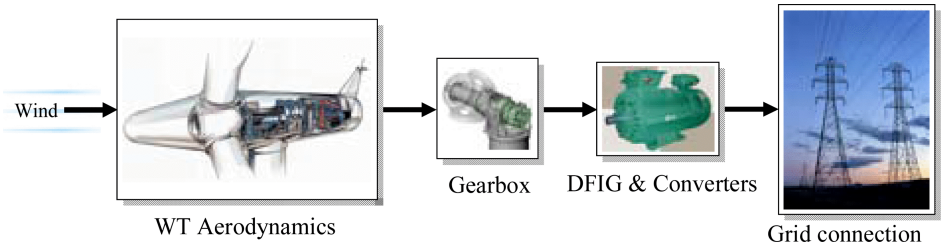

Figure 1.4: Block scheme representing how the system has been implemented [24]

located in a close space, where the wake of a turbine can affect the input wind speed for other turbines

3. The development of a mathematical model for the electrical generator installed on the turbine and the relative power converter and grid connection, where the system is then responsible for the conversion of the mechanical energy into electrical energy

4. The development of control algorithm for the single wind turbine system, considering both the mechanical aspects such as the rotational speed, but also of the electrical system itself and its parameters such as currents.

5. The development of a supervisory control system for the wind farm, responsible for the estimation of the optimal speed target to obtain the best trade-off between power production and mechanical stress on the wind turbines.

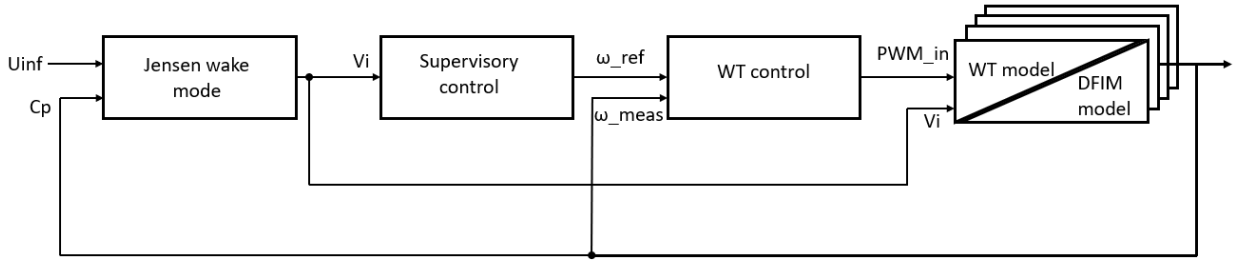

Figure 1.5: General block scheme representing the various research topics and their connections

After an analysis of the current trends for the research, the starting points chosen and assumptions can be summarized as:

1. The input wind speed is assumed known and both in intensity and in direction, and so the wind speed is assumed to come only from one fixed direction.

2. The wind turbines are assumed to be identical, same mechanical/electrical characteristics and same height installment .

3. The wind turbines are all operating in region 2, where the power extracted is proportional to the wind speed, and the pitch angle of blades is considered fixed (explanation in chapter 2).

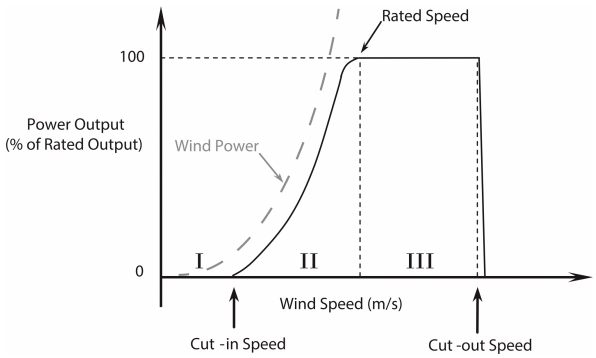

Figure 1.6: Operational regions for a HAWT [2]

4. The wind turbines are assumed to be four, and to be installed in a diamond shape, as shown in Figure 1.7

5. The wind turbines are equipped with doubly induction machines for the electrical energy generation, the power converters are assumed to be composed with ideal switches with no losses.

6. The electrical grid is considered as a three phase-voltage generator with a star connection, and all the turbines are connected in parallel to it.

7. The wind turbine control loops are designed by means of a super-twisting sliding mode control algorithm, defined in the continuous time.

8. All the measurements required by the control loops are assumed measurable without noise.

9. The supervisory control is implemented with the interior point method algorithm.

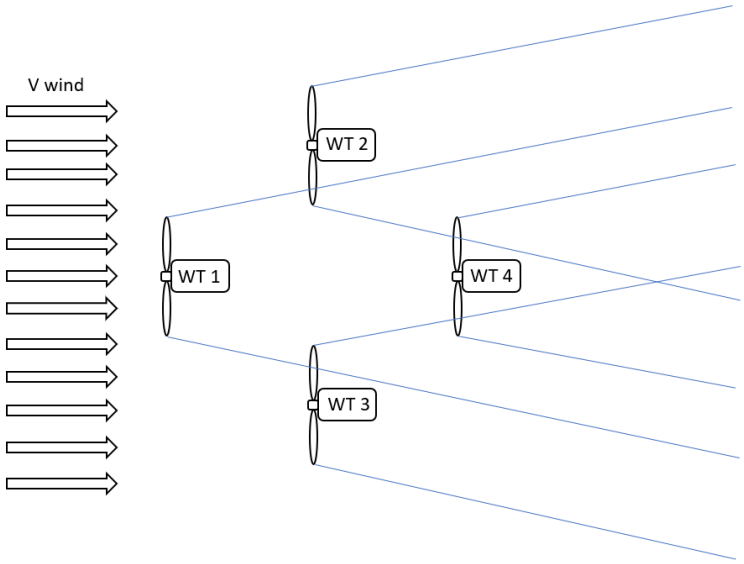

Figure 1.7: Wind turbines composing the wind farm, disposed in a diamond shape layout

Chapter 2

WIND TURBINE AERODYNAMIC MODEL

2.1 Introduction

In this chapter, a description of the physical laws of the aerodynamics of the wind turbines is presented, followed by a description of the MATLAB/Simulink implementation of the two systems. With the same structure, also the modeling of the wake interaction, both for mathematical formulation and MATLAB/Simulink modeling is presented.

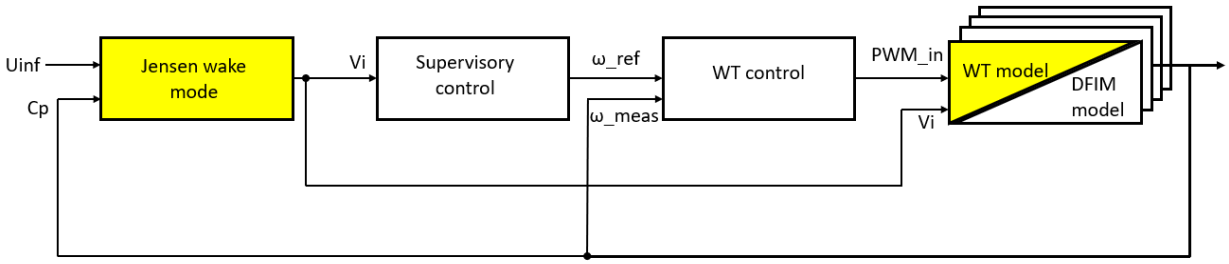

Figure 2.1: Research block scheme: this chapter focuses on the aero-mechanical aspect of the single WT

2.2 Wind turbine structure and components

An Horizontal Axis Wind Turbine (HAWT), as can be senn from Figure 2.2, is composed by a tower, that is a mechanical structure that support the nacelle, that is the second main component, nonetheless, the turbine itself, by means that in the nacelle, are located all the components necessary to convert the wind energy into electrical energy. So after that the wind energy has been captured by the blades, which design and aerodynamics are neglected for this research, a gearbox, multiply the rotational speed of the turbine shaft, in such way that the output speed reaches values of speed that are around the nominal speed of the electrical machine.

Another important component, that again for the purpose of this research has been neglected in the modeling and control of the wind turbine is the braking system. This component is activated when the wind speed, and consequently the thrust on the tower and the rotational

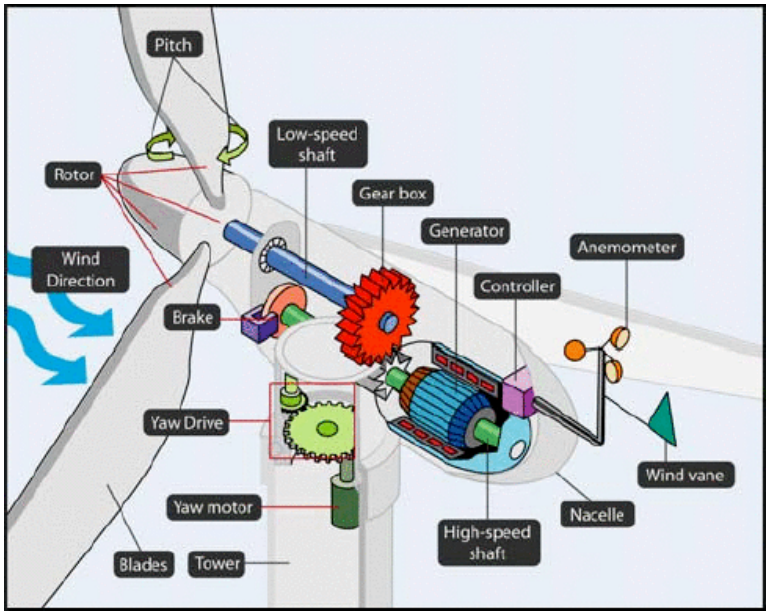

Figure 2.2: Wind turbine main components [1]

speed of the shaft goes over a maximum value. In such way, it's possible to avoid serious mechanical damages to the system.
An important mention can also be done for the pitch control system, which is a complex of hydraulic or electrical actuators used for regulating the pitch angle of the turbine blades, which is the main control action used in region 3, when, as explained in [1], the power of the generator is limited to a constant value after a certain value of wind speed, which normally is equal to the nominal wind speed of the turbine.
The last important component of regulation of the turbine is the yaw control system, which, again by means of hydraulic or electrical actuators, can orientate the turbine is such way that can extrapolate the desired amount of power and at the same time deflecting the wake in such way that the wake interactions between turbines in a wind farm system is lower. This became particularly important when the wind direction is variable or the wind farm is composed by a very compact cluster of turbines.

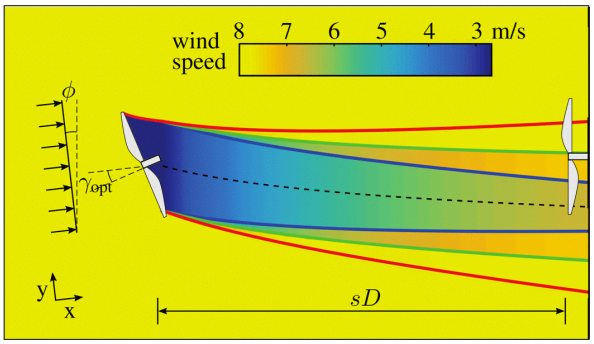

Figure 2.5: Yaw control system [2]

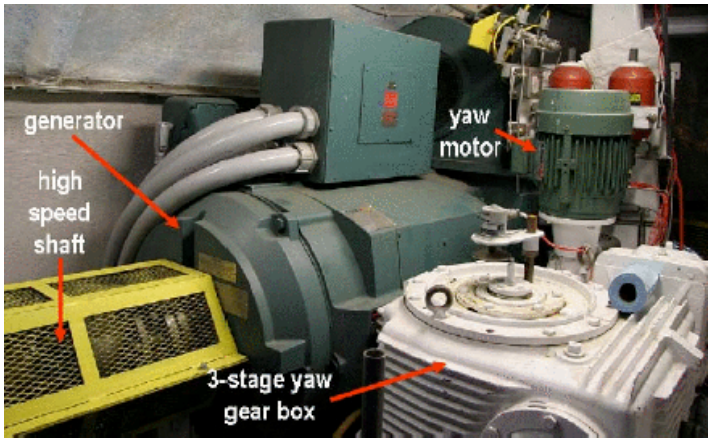

Figure 2.3: Inside the nacelle of a wind turbine [1]

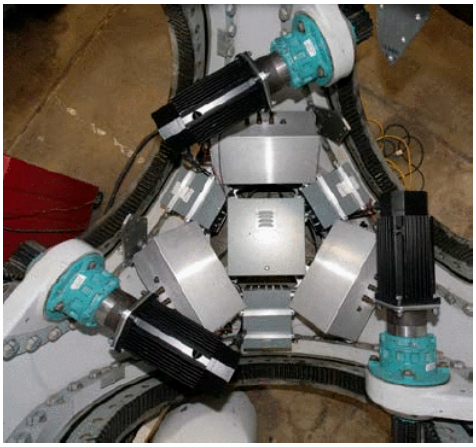

Figure 2.4: Pitch control system [1]

Wind energy and power curves

Depending on the wind speed and direction, a certain control action is implemented. In general, three operational regions can be defined:

1. Region 1, also defined low wind speed region, is an operational situation where the power produced is low compared to the mechanical losses [1], and the turbine consequently is kept un-operating and in brake mode.

2. Region 2, which is the operational region assumed for this research, is when the turbine operates in wind speeds in the range of a minimum value (usually around 7-8 m/s but depends a lot from the turbine) to the base wind speed (around 12-13 m/s). In this region, the main goal is to capture all the possible power available, and considering that this is the region where the generator varies its rotational speed, the main control action implemented is the torque control. That implements the generation of a certain electro-mechanical torque, in opposition to the mechanical torque coming from the wind turbine's blades, in order to regulate the speed at a desired value. The description of the control technique is the argument of chapter 4 of this research.

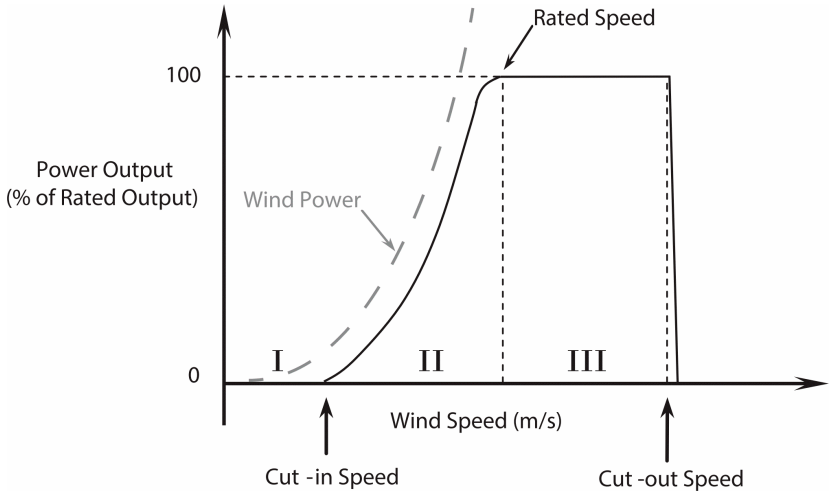

Figure 2.6: Operational regions for a HAWT [2]

3. Region 3, which is the region that comprehends all the values of wind speed from the base wind speed to the maximal accepted value for security before activating the brakes. In this region, as can be seen from figure 2.5, the power production is kept constant, due to keeping the electrical generator working at its rated values, especially for currents. The main control action in this region is the blade pitch angle regulation, where the blades rotates around their axes in order to regulate the drag, and consequently the mechanical power extracted from the wind resource. As mentioned before, the control of the pitch angle, and consequently, the study of the turbine in region 3 is not analyzed in this research, but it is one of the major research topics on the argument on a global scale.

2.3 Fundamentals of wind turbine aerodynamics

The conversion of the kinetic energy from the wind resource to the mechanical energy available to the shaft, can be described starting from the study of the air flow entering in contact with wind turbine's blades. This can be done by means of various detailed models considering different assumptions, but for the purpose of this research it has been chosen as a starting point the wide known Actuator Disk Model, which phenomena is well described in [9] , which is taken as a starting point for this elaborate.

The Actuator Disk Model (ADM), defines the wind turbine's blades complex as a homogeneous porous disk, from which the air flow pass by, and it's characterized by the following assumptions [9]:

1. no frictional drag
2. homogeneous and not compressible fluid, constant air density
3. steady state flow of the fluid
4. constant pressure increment of thrust per unit area over the disk
5. constant pressure increment of thrust per unit area over the disk

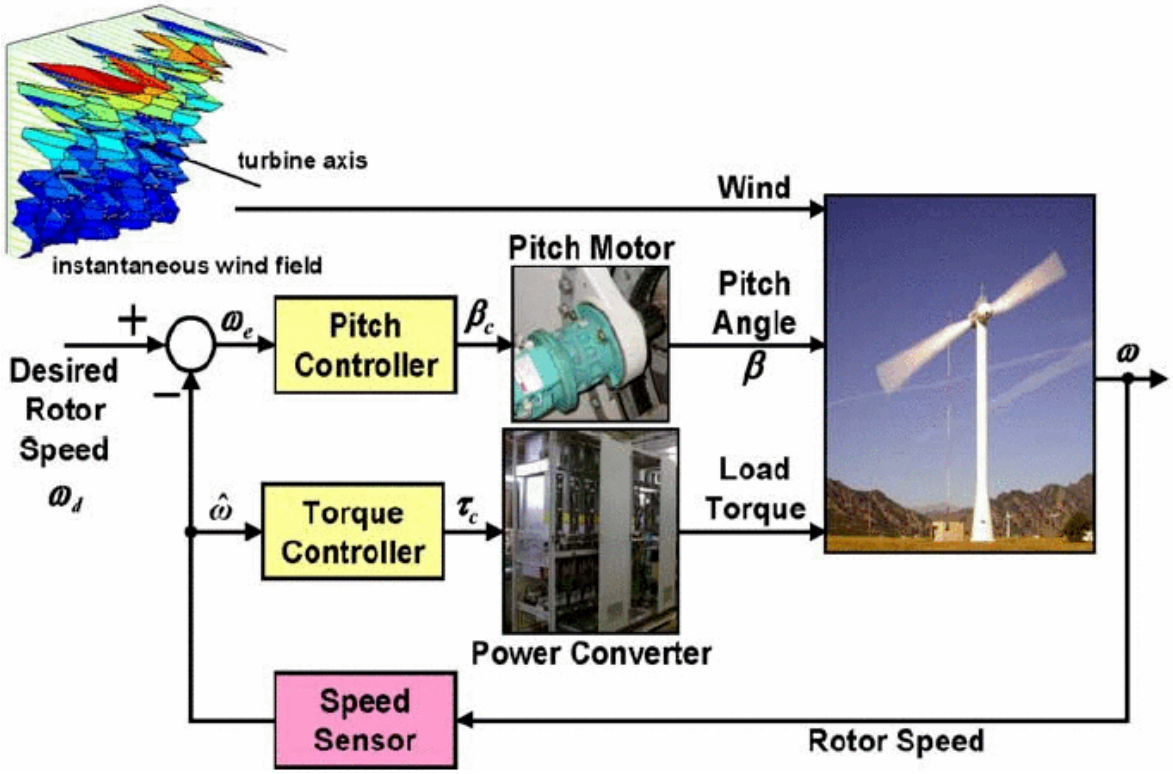

Figure 2.7: Control scheme for a HAWT [1]

6. infinite number of blades

This model of course cannot be utilized for blade's design or detailed studies of wind flows, but it's sufficient for the describing the power and thrust generated by the wind energy conversion.

The ADM's starting point is the study of the air flow by means of the Bernoulli's equation, computed in four main areas of study: free-stream region, just before the blades, just after the blades and the far wake region.

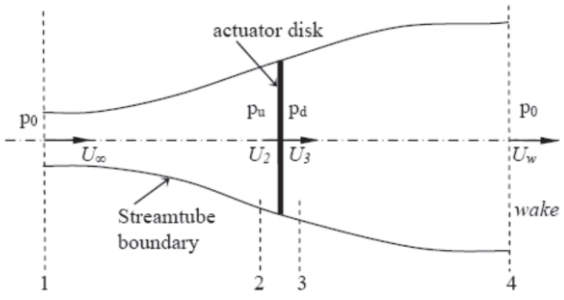

Figure 2.8: Actuator disc model [9]

Writing the Bernoulli's equations for upwind (before the turbine) and for downwind (after the turbine) knowing that:

$$U_2 = U_3 = U_R \tag{2.1}$$

$$p_d + \frac{1}{2}\rho U_R^2 = p_0 + \frac{1}{2}\rho U_w^2 \tag{2.2}$$

$$p_0 + \frac{1}{2}\rho U_\infty^2 = p_u + \frac{1}{2}\rho U_R^2 \tag{2.3}$$

And by knowing that

$$p_0 = p_w$$

and combining (2.2) and (2.3) it's possible to define the pressure drop responsible for the energy extraction

$$p' = \frac{1}{2}\rho(U_\infty^2 - U_w^2) \tag{2.4}$$

From the pressure drop, so by the velocity decrease it's possible to define the Axial Induction Factor, that is defined as the velocity reduction relative to the free wind speed:

$$a = \frac{U_\infty - U_R}{U_\infty} \tag{2.5}$$

From the axial induction factor definition it's possible to define the power coefficient and the thrust coefficient, which are respectively the percentage of power extracted by the wind turbine from the wind resource and the thrust acting on the turbine's nacelle.

$$C_p = 4a(1-a)^2 \rightarrow P = \frac{1}{2}\rho A C_p U^3 \tag{2.6}$$

$$C_T = 4a(1-a) \rightarrow T = \frac{1}{2}\rho A C_T U^2 \tag{2.7}$$

The main idea of the wind energy conversion systems is that the energy extraction from the wind is caused by the capture of the kinetic energy from the wind, which corresponds to a decrease in the wind speed coming out of the turbine. But it's important to remember that there's a limit in the energy extraction, and that value is defined by Betz's law. The Betz's law, which demonstration is omitted here, but well defined in [10], shows that there is maximum value for the power coefficient Cp, to which corresponds a maximum value for the axial induction factor:

$$Cpmax = \frac{16}{27} \approx 0.59 \rightarrow a_{max} = \frac{1}{3}$$

And by remembering that:

$$C_p = 4a(1-a)^2 = \frac{P_{mech}}{P_{wind}} \tag{2.8}$$

this means that the maximum power extracted from a wind turbine cannot be more that 59% of Pw. In reality, as shown later, this value is lower due to un-modeled dynamics and energy losses in the actuator disk model. This limit will be used later in the development of the optimization algorithm for the wind farm.

2.4 Model of a wind turbine

The energy capture, defined by the power coefficient, is also function of how the wind turbine is designed and how the system is controlled, that means that each turbine is characterized by a performance curve [13], that is defined by a non-linear equation:

$$C_P(\lambda, \beta) = 0.22 \left(\frac{116}{\kappa_i} - 0.4\beta - 5 \right) e^{\frac{-12.5}{\kappa_i}} \tag{2.9}$$

where the numerical coefficient:

$$\frac{1}{\kappa_i} = \frac{1}{\lambda + 0.08\beta} - \frac{0.035}{\beta^3 + 1} \tag{2.10}$$

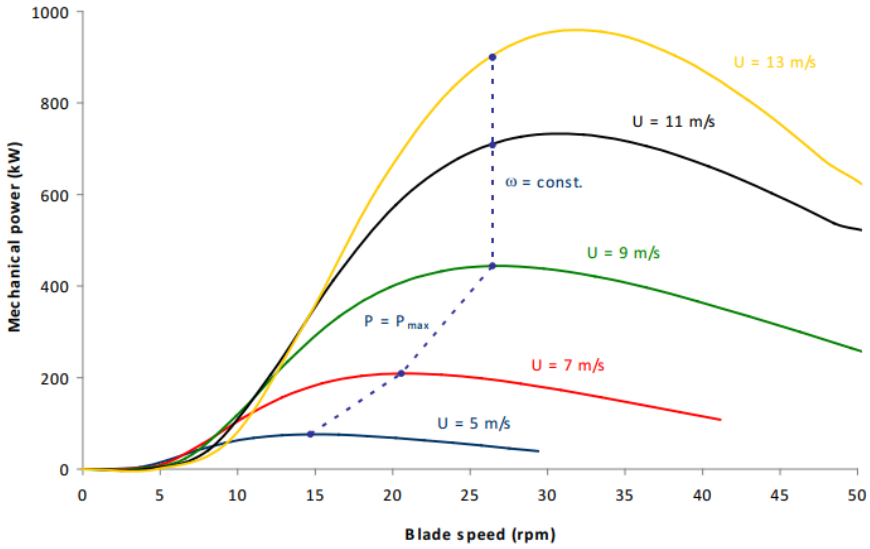

Figure 2.9: Example of Power coefficient curves versus rotational speed for various wind speeds [13]

and where lambda is defined as the tip speed ratio:

$$\lambda = \frac{\omega R}{V} \tag{2.11}$$

where ω is the rotational speed of the turbine shaft, R is the radius(length) of the turbine blades and V is the input wind speed, and where beta is the pitch angle, that is the angle for which the turbine's blades are rotated.

The values of the coefficients in (2.9) depends on the wind turbine design, while instead

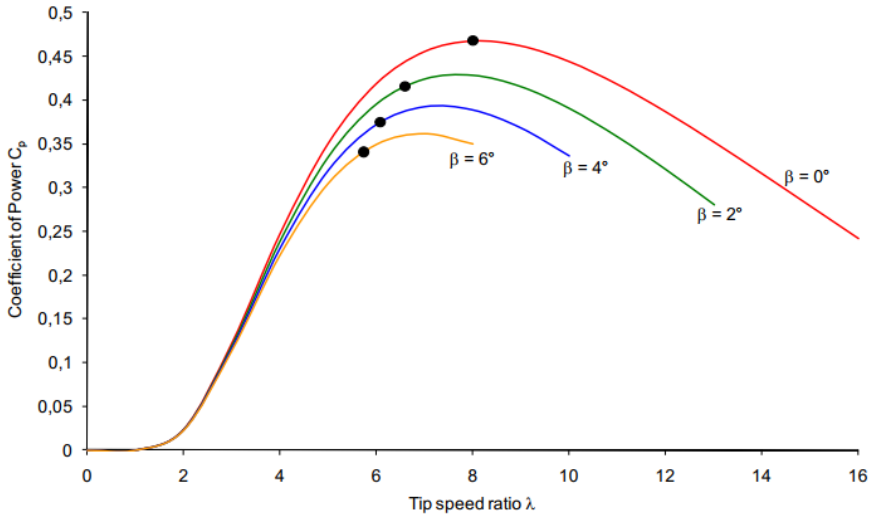

Figure 2.10: Example of Power coefficient curves versus tip-speed ratios for various β[13]

lambda and beta are control parameters for speed regulation and power production.

As can be seen from figure 2.11, the block scheme for the model of the wind turbine implements the equations 2.11, 2.9 and 2.6, and, as explained in the first chapter, the pitch angle is assumed constant during the simulations. The final output for this subsystem is the mechanical torque produced from the wind energy capture and conversion. This torque is applied, through a drive train, to the shaft of the electrical machine.

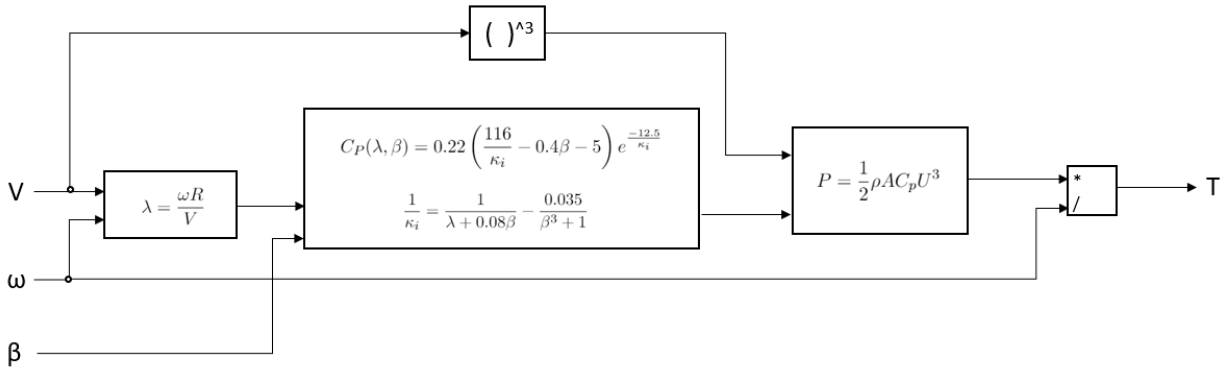

Figure 2.11: HAWT's block scheme

In order to design a simple and manageable model for the project, it has been chosen to directly use the Simscape's component for the wind turbine. This, with difference from the one explained before, works with pu measurements, so in order to implement it with the generator it was necessary to apply some unit conversions. As can be seen from figure 2.12, the block still receive the wind speed and the pitch angle in SI units, but the the rotational speed, needs to be converted in terms of pu measurements. So it has been divided by the nominal speed of the generator, and after that by the gear ratio of the drive train.

WT's Parameter	Symbol	Value	Unit measure
Radius	R	100	[m]
Air density	ρ	1.225	[kg/m^3]
Pitch angle	β	0.5	[° degrees]
Nominal rotational speed (DFIG shaft)	ω_n	1500	[rpm]
Gear ratio	N	10	[/]
Nominal power coefficient	Cp$_{nom}$	0.48	[/]
Nominal tip speed ratio	λ_n	8.1	[/]
Nominal rotational speed (pu)	speed$_n$	1.5	[/]
Base wind speed	V$_{wind}$	13	[m/s]
Nominal power (pu)	P$_N$	0.73	[/]
Base wind power	P$_{wind}$	2e6	[W]
Base electrical power	P$_n$	2e6/0.9	[W]

Table 2.1: Wind turbine model's parameters and relative values

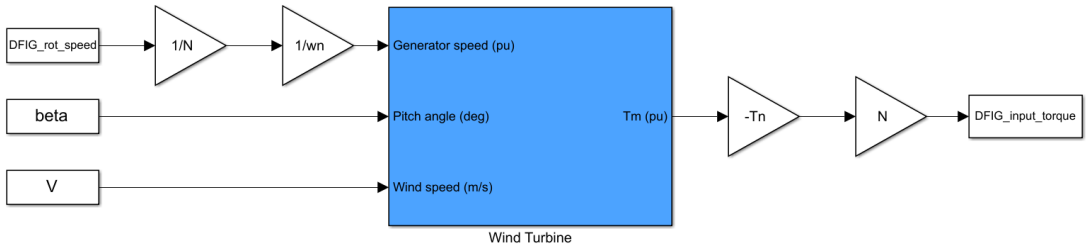

Figure 2.12: Implementation of the HAWT in Simulink [MATLAB]

One thing that can be noticed for the drive train is that, it has been modeled by a simple gear ratio constant, neglecting dampings and stiffness. The inertia of the blades has also been neglected in order to obtain a simpler model.
The mechanical torque in output, needed to be converted again to the low speed gear, but more importantly to the SI unit. It has been assumed, again for simplicity, that the nominal torque of the wind turbine is equivalent to the nominal torque of the generator.

2.5 Wake definition and characteristics

As explained in [2], the output wind by which the turbine has extracted energy is characterized by a change in the wind flow, and this alteration is defined as the wake of the turbine. This wake is characterized by:

1. wind velocity reduction, as a consequence of the energy extraction
2. increase in turbulence intensity, due to the rotation of the turbine's blade's effect on the wind
3. wake expansion, as described by the law of mass conservation assuming an not compressible fluid

There are also other effects and characteristics of a wake, such as deflection and wake recovery, but in the developed model are not considered, and so consequently not treated in this elaborate.

During the course of the years, many wake models have been developed, and a review of those models can be found in [7]. The models have been developed in function of the studies done on the wind turbine systems, there are kinematic models, which are simpler but that require less computational power and time, and there are flow field models, that are more detailed but that require more computational power and time. Those last one are usually used for CFD simulations and used for blade design and aerodynamic studies.

	Low fidelity		**Medium fidelity**	**High fidelity**
Model type	Kinematic models		Flow field models	Flow field models
Funda-mentals	Parametric		2D NS	3D NS
Models	Jensen, FLORIS, Frandsen, ...	FLORI-Dyn,...	DWM, WFSim, Ainslie...	SOWFA, WakeFarm, UTDWF, SP-Wind,...
Flow dimension	2D		2D	3D
Dy-namic/Static	Static	Dynamic	Dynamic	
Turbine model	ADM		ADM/ALM and/or an aerodynamic package (e.g., FAST)	
Comp. effort	Order of seconds on a desktop PC		Order of minutes on a desktop PC	Order of days on a cluster of 10^2 CPUs
Model accuracy	Low – medium		Medium – high	High – very high

Figure 2.13: Classification of the wake models [2]

In order to develop a model of wind farm and the wake interactions between turbines, a simple kinematic model, which is one of the standards in the research field, has been chosen for this research.
The wake model chosen for this research is known as the Jensen/Park model, developed in the 1980s by N.O. Jensen [6], is a kinematic, parametric, static model developed starting from the actuator disk model theory, which is characterized by a linear expansion of the wake and by a superposition effect of multiple wakes acting on a certain turbine receiving the input wind affected by them. A good description of the model used in this research can be found in [4] and [11].

Starting from (2.5) can be derived that

$$\frac{v_1}{v_0} = (1 - 2a) = \sqrt{1 - C_T} \tag{2.12}$$

So the actuator disk model provides the simplest wake model possible. From this starting point, and assuming the linear expansion, it can be written that

$$r = r_0 + \alpha x \tag{2.13}$$

where, as explained in [4] alpha, defined as the decay coefficient is set to 0.075 for onshore, and to 0.05 for offshore wind farms [5], noticing that alpha = sin(angle of spread of the wake).

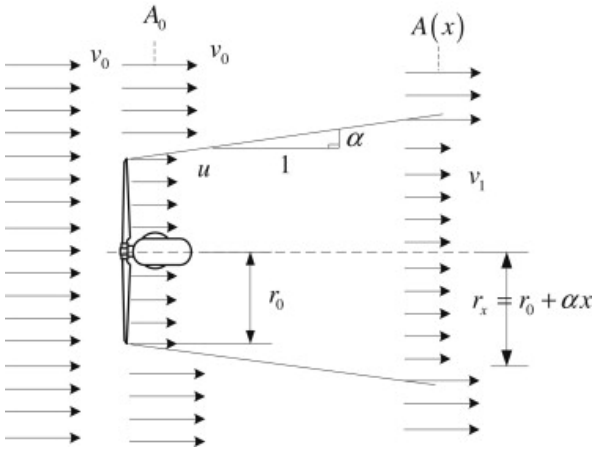

Figure 2.14: Linear expansion of the wake assumed in the Jensen wake model [4]

So the velocity of the wind in the wake at distance x from the turbine can be computed as

$$v_1 = v_0 + v_0(\sqrt{1 - C_T} - 1)\left(\frac{r_0}{r}\right)^2 \tag{2.14}$$

This formula still not includes effects of multiple wakes or a partial shadowing of the turbine receiving the input wind speed affected by wakes.

As assumption, for simplicity of the mathematical formulation, all the turbines considered have the same radius, exactly as described before, and so for the entire research. By using trigonometric relationships we can define the shadowing area, that is the intersection between the area of the wake entering in input to a certain turbine and the circular area of that precise turbine, such as:

$$A_{sh,i} = [r_i(x_{ij})]^2 cos^{-1}\left(\frac{L_{ij}}{r_i(x_{ij})}\right) + r_0^2\left(\frac{d_{ij} - L_{ij}}{r_i(x_{ij})}\right) - d_{ij}z_{ij} \tag{2.15}$$

where

$$z_{ij} = \frac{1}{d_{ij}} \sqrt{4(d_{ij}^2)(r_{ij}^2) - (d_{ij}^2 - r_0^2 + r_{ij}^2))} \tag{2.16}$$

where d_{ij} is the x-axis relative distance between the turbines i and j.

$$L_{ij} = d_{ij}^2 - r_0^2 + r_{ij}^2 2 d_{ij} \tag{2.17}$$

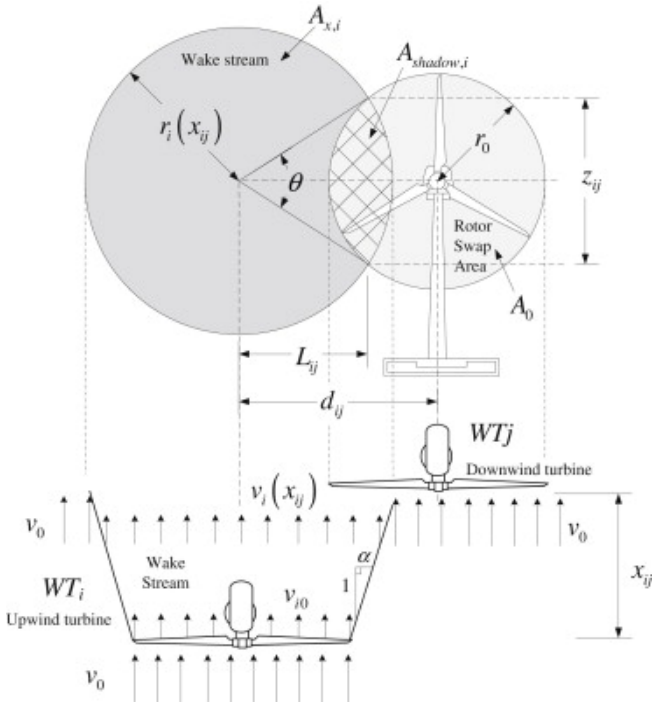

Figure 2.15: Effect and parameters of partial shadowing [4]

Consequently, applying the superposition effect, by which the total effect of the wakes, it's the sum of the single wake effects, the complete model for the input wind speed of a turbine is:

$$v_j(x_{ij}) = U_\infty \left[1 - \sum \left(1 - \sqrt{1 - C_T} \left(\frac{r_0}{r_i(x_{ij})} \right)^2 \frac{A_{shadow,i}}{A_0} \right) \right] \tag{2.18}$$

In our system, the number of wind turbines and the layout of the wind farm are known, so the wake interactions between turbines are known a priori. In this particular case, it's possible to write a fixed formula for every turbine, instead of developing an algorithm.

$$v_1 = U_{inf} \tag{2.19}$$

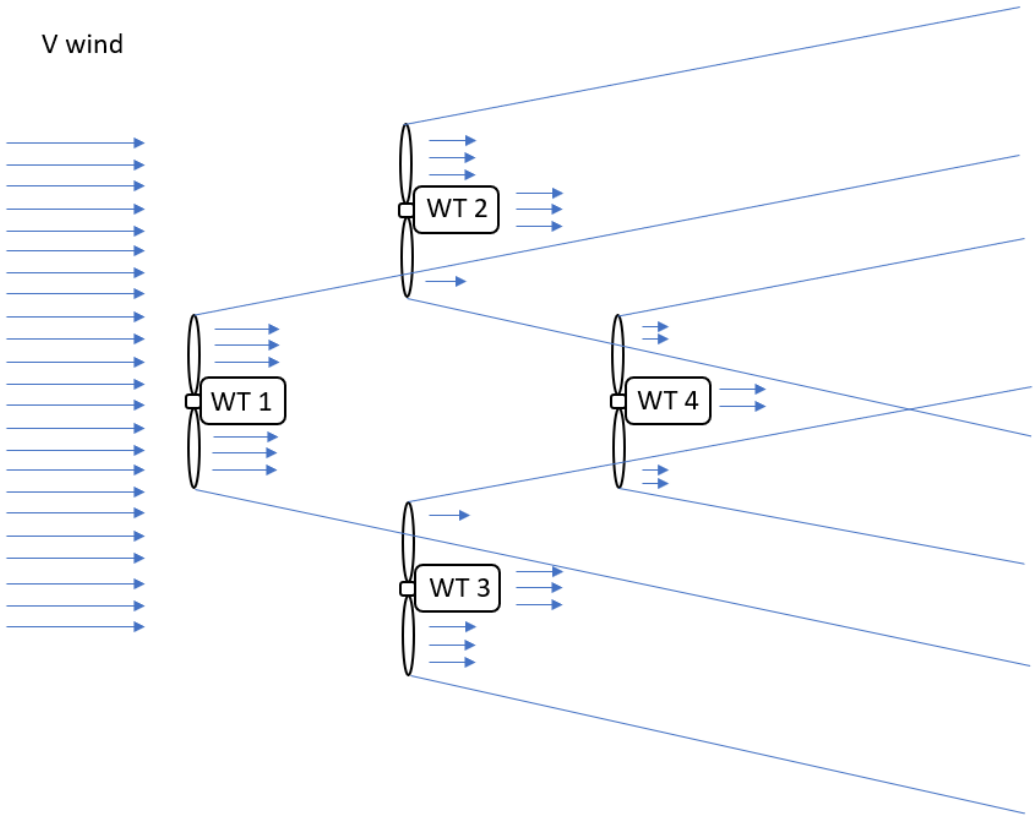

Figure 2.16: Shadowing effect in a diamond shape wind farm

Of course the first turbine does not have any wake interaction, because by being the first turbine in the system, it receives the free wind input.

$$v_2 = U_{inf}(1 - (1 - \sqrt{1 - C_{T2}}) \left(\frac{r_0}{r_{12}}\right)^2 \frac{A_{sh_{12}}}{A_0} \tag{2.20}$$

$$v_3 = U_{inf}(1 - (1 - \sqrt{1 - C_{T3}}) \left(\frac{r_0}{r_{13}}\right)^2 \frac{A_{sh_{13}}}{A_0} \tag{2.21}$$

Turbine 2 and 3 are subject to a partial shadowing caused by Turbine 1.

$$v_4 = U_{inf} \left(1 - (1 - \sqrt{1 - C_{T4}}) \left(\left(\frac{r_0}{r_{14}}\right)^2 \frac{A_{sh_{14}}}{A_0} + \left(\frac{r_0}{r_{24}}\right)^2 \frac{A_{sh_{24}}}{A_0} + \left(\frac{r_0}{r_{34}}\right)^2 \frac{A_{sh_{34}}}{A_0}\right)\right) \tag{2.22}$$

Turbine 4 instead is subject to a partial shadowing caused by all the other turbines.

In order to implement the wake model in such way that the wind velocity enters as input for each wind turbine block, it was chosen such design:

The MATLAB function block implement the relations described before for each turbine, considering for each turbine all the turbines in front of them. Values for positions and dimen-

sions where chosen for the only purpose of testing, and are not based on a specific case. More detail about code implementation of the model can be found in Appendix.

Chapter 3

WIND TURBINE ELECTRO-MECHANICAL MODEL

In this chapter, a simplified explanation of the mathematical concepts and physical laws regarding the technology of the doubly fed induction machine is presented. Its use in the wind energy production, the relative electrical drive scheme and its implementation in MATLAB/Simulink is also described.

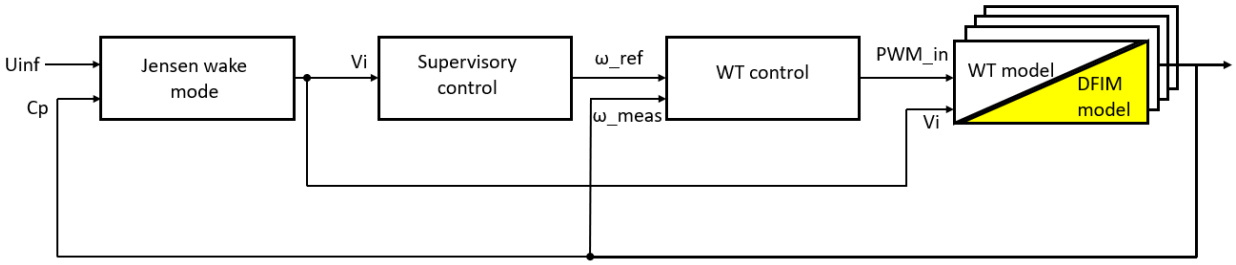

Figure 3.1: Research block scheme: this chapter focuses on the electrical aspect of the single WT

3.1 Introduction

In the wind energy field, many kind of electrical machines and drives are implemented for energy production, but the most used nowadays is the doubly fed induction generator (DFIG), due to many advantages, well described in [16]. The main characteristic of this machine is the ability to work as a generator both in sub-synchronous and in super-synchronous modes thanks to the control done by means of the back-to-back converter, as explained later on.

This capability becomes very important considering the variability of the wind speed due to its intrinsic aleatory nature. Another important consideration is the fact that the rotational speed variations are always around the synchronous speed of the stator's rotating magnetic field, and so the converter dimensioning can be reduced, typically at the 30% of the nominal power [15].

The doubly-fed induction machine is characterized by having both the stator and the rotor built with windings. In this way, it is possible to connect the machine with two different parts

of the system.

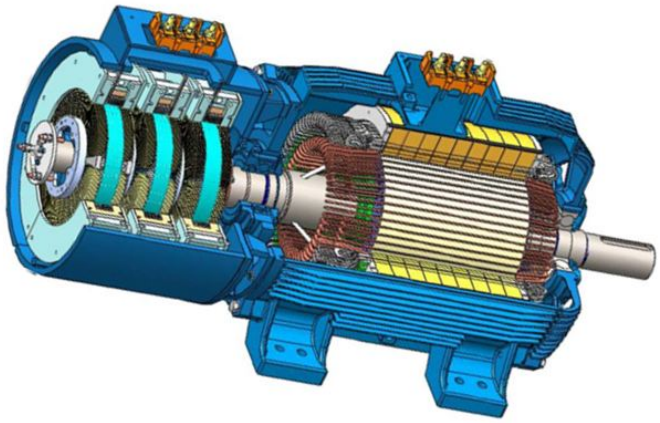

Figure 3.2: View of a doubly-fed induction machine with rotary transformer [19]

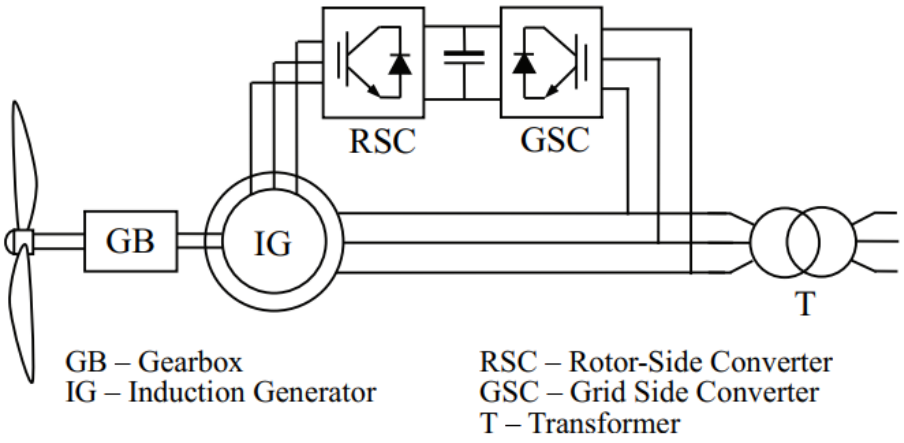

Figure 3.3: Schematic of the typical DFIG's main components and relative configuration [15]

As can be seen in Figure 3.3 the typical arrangement consists of the direct link between the stator windings and the grid, creating the stator magnetic field with constant amplitude, frequency and phase. The rotor windings are instead attached to the AC side of the rotor side converter (RSC), that creates three phase voltages with variable amplitude and frequency in order to control torque, speed and power of the electrical machine.

3.2 Reference transformations

In order to design a control system and analyze transient behaviours that happens in the electrical machine, it is necessary to define a dynamic model that consider the variations of magnetic fluxes, and consequently of the currents.

But describing a dynamic model in a three phase reference system, generates complex equations that are hard to understand intuitively and requires a considerable amount of computational power. So instead, it is common practice to define new reference frames.

The first transformation done is the passage from a three phase domain to a two-phase domain, where the system is described in two axis with a 90° angle between them, but this new reference frame is still fixed in space, with the same referring point of the three phase system. The system described is constituted by two sinusoidals (voltages, currents or fluxes) oscillating with the same frequency of before.

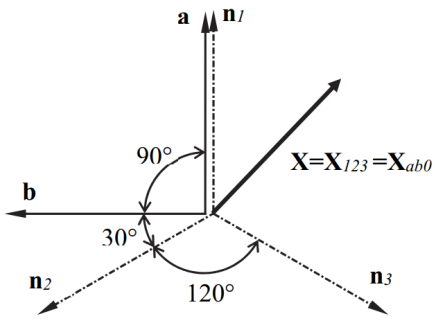

Figure 3.4: Geometrical representation of 3-axis and 2-axis reference frames at comparison [20]

The transformation T responsible for transforming from a three-phase system (abc) to a two-phase system (alpha-beta) and the inverse for the opposite transformation are defined as [20]:

$$T = \begin{bmatrix} \sqrt{2/3} & -1/\sqrt{6} & -1/\sqrt{6} \\ 0 & 1/\sqrt{2} & -1/\sqrt{2} \\ 1/\sqrt{3} & 1/\sqrt{3} & 1/\sqrt{3} \end{bmatrix} \quad T^{-1} = \begin{bmatrix} \sqrt{2/3} & 0 & 1/\sqrt{3} \\ -1/\sqrt{6} & 1/\sqrt{2} & 1/\sqrt{3} \\ -1/\sqrt{6} & -1/\sqrt{2} & 1/\sqrt{3} \end{bmatrix} \tag{3.1}$$

But still, in the alpha-beta reference frame, we are still dealing with sinusoidal parameters for which creating a control system can be difficult in terms of mathematical modeling. What can be done is to describe the electrical equations in a new reference frame that rotates synchronously with the rotor shaft.
The transformation T responsible for transforming from a fixed two-phase system (alpha-beta) to two-phase system (dq) and the inverse for the opposite transformation are defined as [20]:

$$R_\theta = \begin{bmatrix} \cos\theta & \sin\theta \\ -\sin\theta & \cos\theta \end{bmatrix} \quad R_\theta^{-1} = \begin{bmatrix} \cos\theta & -\sin\theta \\ \sin\theta & \cos\theta \end{bmatrix} \tag{3.2}$$

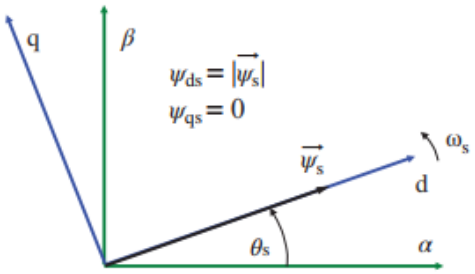

Figure 3.5: Geometrical representation of fixed and rotating 2-axis reference frames at comparison [14]

3.3 Doubly Fed Induction Machine

3.3.1 Steady state

Before describing the control scheme for the DFIM, it is necessary to describe, at least in a synthetic way, the fundamental laws describing the behaviour of the electrical machine itself. The starting point is the relationship between the magnetic field at the stator (constant in amplitude and frequency) and the magnetic field at rotor and the rotational speed of the rotor itself. In fact, the DFIM is by definition an asynchronous machine, which means that the magnetic field of the stator and the rotational speed of the rotor are not the same. Another good description of the phenomenon can be found in [15], while the the equations describing the behaviour of the electrical machine are taken from [14].

This difference of speed is compared while looking at the electrical speed of the shaft, which by definition depends by the number of poles in the machine:

$$\omega_m = p\Omega_m \tag{3.3}$$

So the most important coefficient in the asynchronous machine is the slip, which represents the relative variation of speed between the stator magnetic field and the rotor itself:

$$s = \frac{\omega_s - \omega_m}{\omega_s} \tag{3.4}$$

Depending on the sign of the slip, the asynchronous machine is said to be in one of three possible operating modes:

$$\begin{cases} \omega_m < \omega_s \Rightarrow s > 0 \quad \Rightarrow \quad \textit{Sub synchronous operation} \\ \omega_m > \omega_s \Rightarrow s < 0 \quad \Rightarrow \quad \textit{Super synchronous operation} \\ \omega_m = \omega_s \Rightarrow s = 0 \quad \Rightarrow \quad \textit{Synchronous operation} \end{cases}$$

Normally, the asynchronous machine operates as generator while in super-synchronous mode and as motor in sub-synchronous mode, while instead in synchronous operation the machine produces no torque.

An important factor in the design of the machine and in its modeling, is the ratio between the winding turns of the stator wrt to the rotor's one:

$$u = \frac{N_s}{N_r} \tag{3.5}$$

To describe the relationships between the electrical dynamic of both stator and rotor, an equivalent single phase circuit is created and all the parameters are referred to the stator:

$$R_r = R'_r u^2 \quad L_{\sigma r} = L'_{\sigma r} u^2 \quad \underline{I}_r = \frac{\underline{I}'_r}{u} \quad \underline{V}_r = \underline{V}'_r u \quad \underline{E}_{rs} = \underline{E}'_{rs} u \quad \underline{E}'_{rs} = s\frac{E_s}{u} \tag{3.6}$$

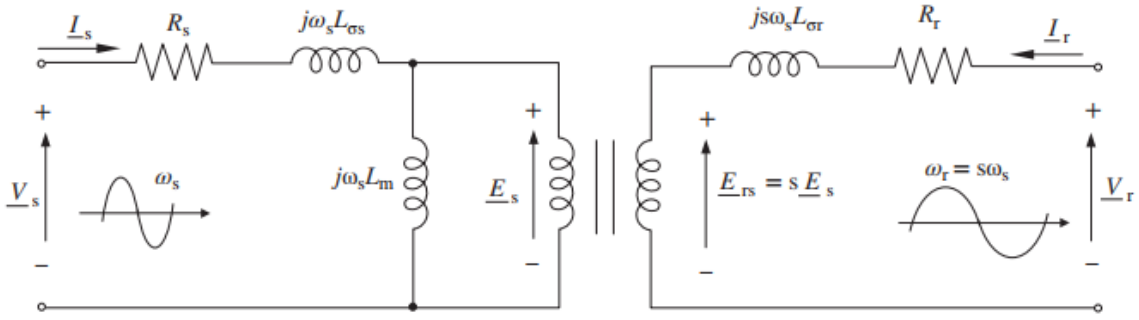

Figure 3.6: One-phase steady-state DFIM equivalent circuit with rotor's parameters reduced to the stator [14]

$$\underline{V}_r - s\underline{E}_s = (R_r + js\omega_s L_{\sigma r})\underline{I}_r \quad \Rightarrow \quad \frac{\underline{V}_r}{s} - \underline{E}_s = (\frac{R_r}{s} + js\omega_s L_{\sigma r})\underline{I}_r \tag{3.7}$$

Consequently, the electric equations of the steady state circuit in the final form are:

$$\underline{V}_s = R_s\underline{I}_s + jsL'_{\sigma s}\underline{I}_s + js\omega_s L_m(\underline{I}_s + \underline{I}_r) \tag{3.8}$$

$$\frac{\underline{V}_r}{s} = \frac{R_r}{s}\underline{I}_r + jsL'_{\sigma s}\underline{I}_r + js\omega_s L_m(\underline{I}_s + \underline{I}_r) \tag{3.9}$$

Similarly for the fluxes:

$$\underline{\Psi}_s = L_m(\underline{I}_s + \underline{I}_r) + L_{\sigma s}\underline{I}_s = L_s\underline{I}_r + L_m\underline{I}_r \tag{3.10}$$

$$\underline{\Psi}_r = L_m(\underline{I}_s + \underline{I}_r) + L_{\sigma r}\underline{I}_r = L_m\underline{I}_s + L_r\underline{I}_r \tag{3.11}$$

where $L_s = L_m + L_{\sigma s}$ *and* $L_r = L_m + L_{\sigma r}$.

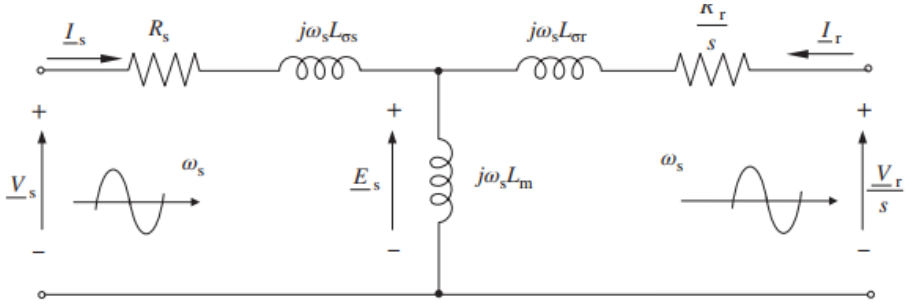

Figure 3.7: One-phase steady-state DFIM equivalent circuit wrt the stator [14]

A simple relation describing the power flows in the machine:

$$P_s + P_r = P_{cu-s} + P_{cu-r} + P_m \tag{3.12}$$

Finally, the definition of the torque in the steady-state domain:

$$T_{em} = \frac{3p}{s\omega_s}[R_r|\underline{I}_r|^2 - |\underline{V}_r||\underline{I}_r|\cos\phi] \tag{3.13}$$

The torque is the variable responsible for the speed control and the power generation of the electrical machine. But developing control algorithms in the three-phase domain is complex and time consuming. So in order to simplify the system description, a transformation of the reference frame is done through two passages.

3.3.2 Dynamic model

After applying the transformation of the reference system T of (3.1), the electrical equations of the asynchronous machine described in the fixed two-phase reference frame and the relative equivalent circuit are:

Stator voltages:

$$\begin{cases} v_{\alpha s} = R_s i_{\alpha s} + \frac{d\Psi_{\alpha s}}{dt} \\ v_{\beta s} = R_s i_{\beta s} + \frac{d\Psi_{\beta s}}{dt} \end{cases} \tag{3.14}$$

Rotor voltages:

$$\begin{cases} v_{\alpha r} = R_r i_{\alpha r} + \frac{d\Psi_{\alpha r}}{dt} + \omega_m \Psi_{\beta r} \\ v_{\beta r} = R_r i_{\beta r} + \frac{d\Psi_{\beta r}}{dt} - \omega_m \Psi_{\alpha r} \end{cases} \tag{3.15}$$

Stator fluxes:

$$\begin{cases} \Psi_{\alpha s} = L_s i_{\alpha s} + L_m i_{\alpha r} \\ \Psi_{\beta s} = L_m i_{\beta r} + L_s i_{\beta s} \end{cases} \tag{3.16}$$

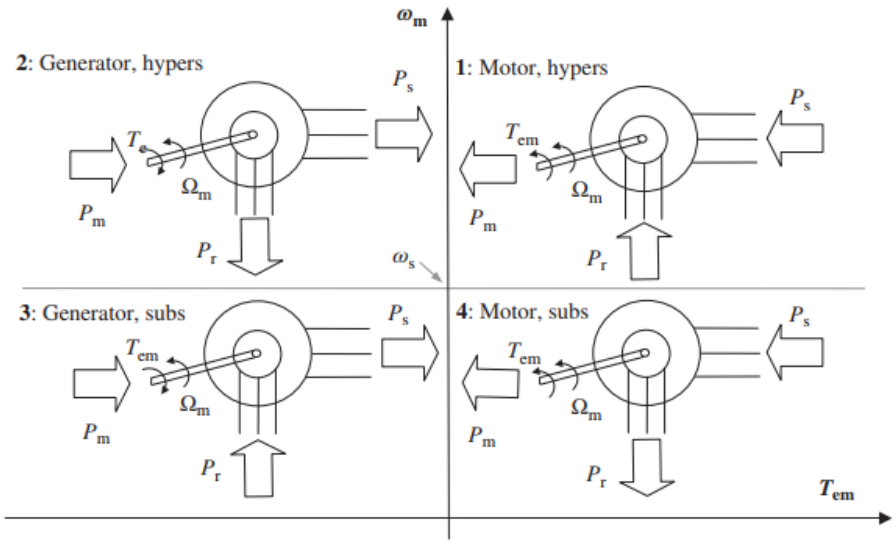

Figure 3.8: Operating modes of the DFIM considering torque sign and speed under/over the synchronous value [14]

Rotor fluxes:

$$\begin{cases} \Psi_{\alpha r} = L_s i_{\alpha r} + L_m i_{\alpha s} \\ \Psi_{\beta r} = L_m i_{\beta s} + L_s i_{\beta r} \end{cases} \tag{3.17}$$

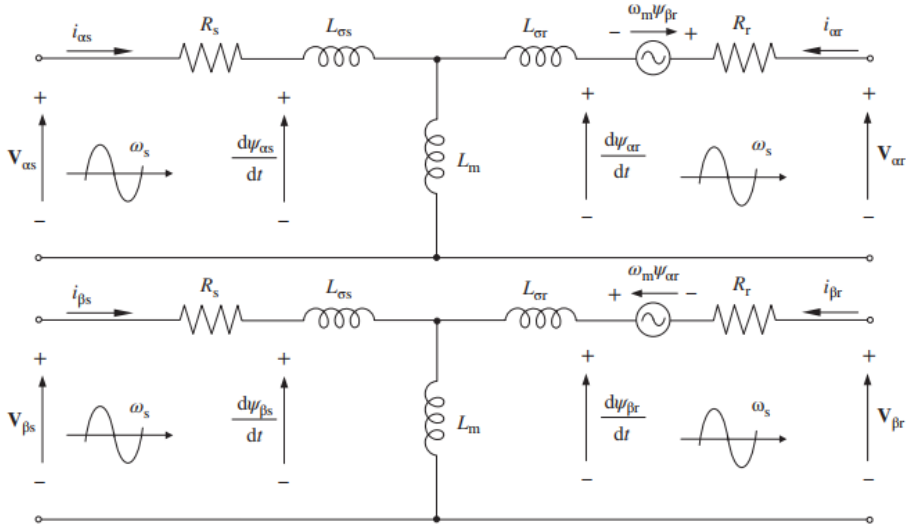

Figure 3.9: DFIM's equivalent circuit in the alpha/beta reference frame [14]

Finally, by applying on the previous two-phase model the reference transformation R of (3.2), the electrical equations of the asynchronous machine described in the two phase rotating reference frame and the relative equivalent circuit are:

Stator voltages:

$$\begin{cases} v_{ds} = R_s i_{ds} + \frac{d\Psi_{ds}}{dt} + \omega_m \Psi_{qs} \\ v_{qs} = R_s i_{qs} + \frac{d\Psi_{qs}}{dt} + \omega_m \Psi_{ds} \end{cases} \tag{3.18}$$

Rotor voltages:

$$\begin{cases} v_{dr} = R_r i_{dr} + \frac{d\Psi_{dr}}{dt} + \omega_m \Psi_{qr} \\ v_{qr} = R_r i_{qr} + \frac{d\Psi_{qr}}{dt} - \omega_m \Psi_{dr} \end{cases} \tag{3.19}$$

Stator fluxes:

$$\begin{cases} \Psi_{ds} = L_s i_{ds} + L_m i_{dr} \\ \Psi_{qs} = L_m i_{qr} + L_s i_{qs} \end{cases} \tag{3.20}$$

Rotor fluxes:

$$\begin{cases} \Psi_{dr} = L_r i_{\alpha r} + L_m i_{\alpha s} \\ \Psi_{qr} = L_m i_{\beta s} + L_r i_{\beta r} \end{cases} \tag{3.21}$$

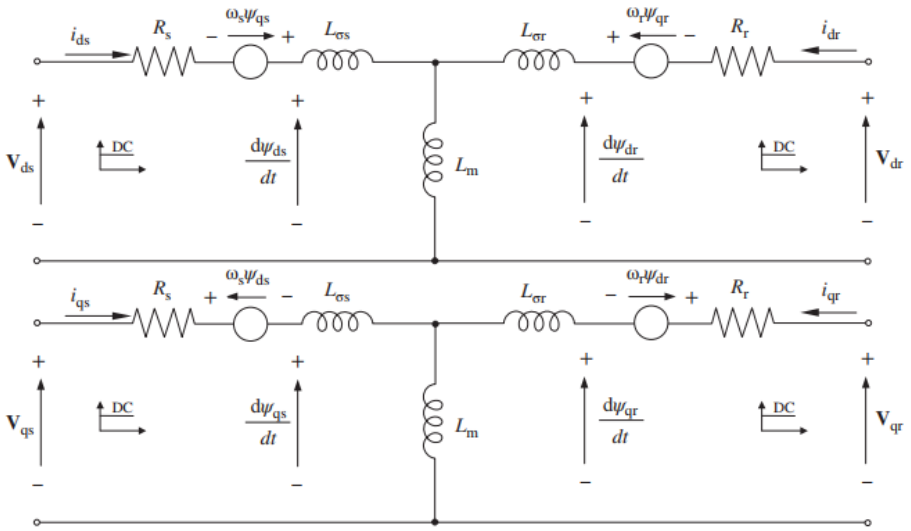

Figure 3.10: DFIM's equivalent circuit in the dq reference frame [14]

3.4 Grid side system

In similar way, the grid system has to be modeled in order to properly design the control system for the grid side converter, starting from the steady state 3-phase model, through the reference transformation we'll arrive to model defined in the dq reference frame from which the control algorithm will be defined.

3.4.1 Steady state model

Following the research done in [18], the grid system is modeled as three voltage sources in a star configuration, this simple representation neglects many aspects of a real grid system, but for the purpose of this research, is sufficient to say that the grid voltage is constant due to the proportion of its power compared to what is produced by the wind farm.
The power converter, that will be described more in detail in the next section, is modeled as

three variable voltage generators, and between them, a simple inductive filter with a parasitic resistance is applied. The entire system can be seen in figure Figure 3.11. As for many

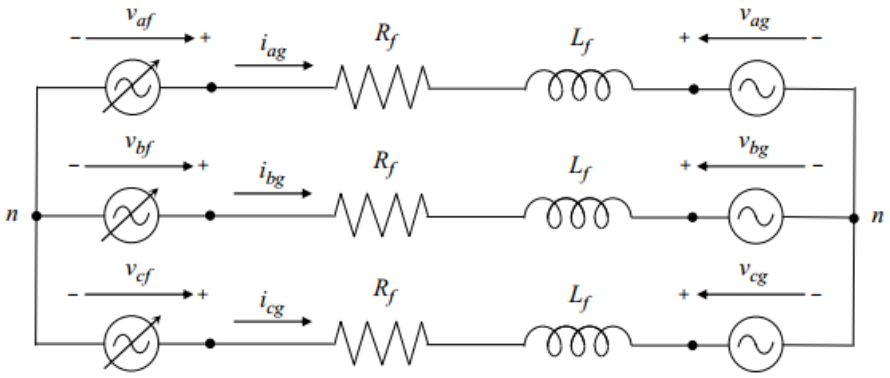

Figure 3.11: Grid side system's equivalent circuit in 3-phase domain [18]

application of three phase system, a single phase equivalent circuit, shown in Figure 3.12 and equation can be modeled:

$$v_{af} = v_{ag} + (R_f + jL_f\omega_s)i_{ag} \tag{3.22}$$

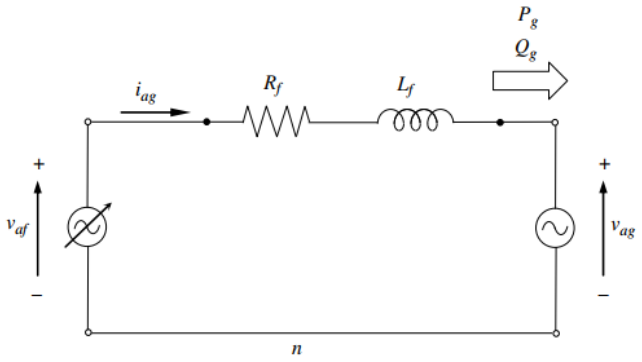

Figure 3.12: Grid side system's equivalent circuit in single-phase domain [18]

3.4.2 Dynamic model

By passing from a three-phase reference system to a two-phase reference system, the voltage equations of the grid side system become:

$$\begin{cases} v_{\alpha f} = R_f i_{\alpha g} + L_f \frac{di_{\alpha g}}{dt} + v_{\alpha g} \\ v_{\beta f} = R_f i_{\beta g} + L_f \frac{di_{\beta g}}{dt} + v_{\beta g} \end{cases} \tag{3.23}$$

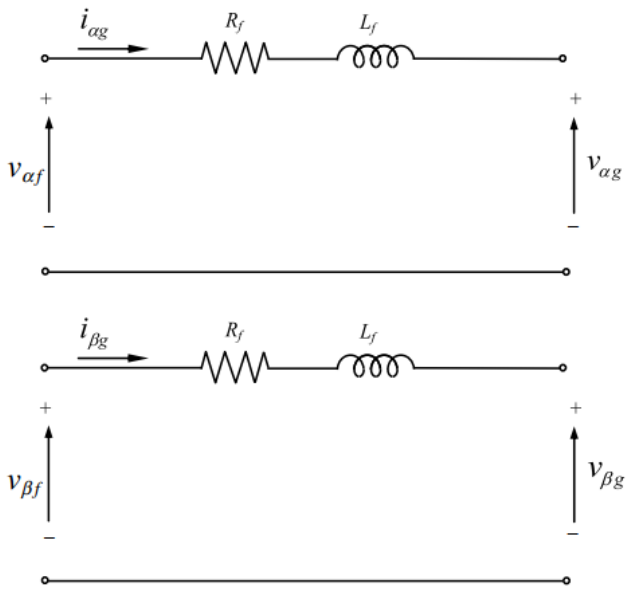

Figure 3.13: Grid side system's equivalent circuit in the alpha/beta reference frame [18]

As for the DFIM, in order to perform the vector control, it's still necessary to convert the system into a rotationary reference frame:

$$\begin{cases} v_{df} = R_f i_{dg} + L_f \frac{di_{dg}}{dt} + v_{dg} - \omega_a L_f i_{qg} \\ v_{qf} = R_f i_{qg} + L_f \frac{di_{qg}}{dt} + v_{qg} + \omega_a L_f i_{dg} \end{cases} \tag{3.24}$$

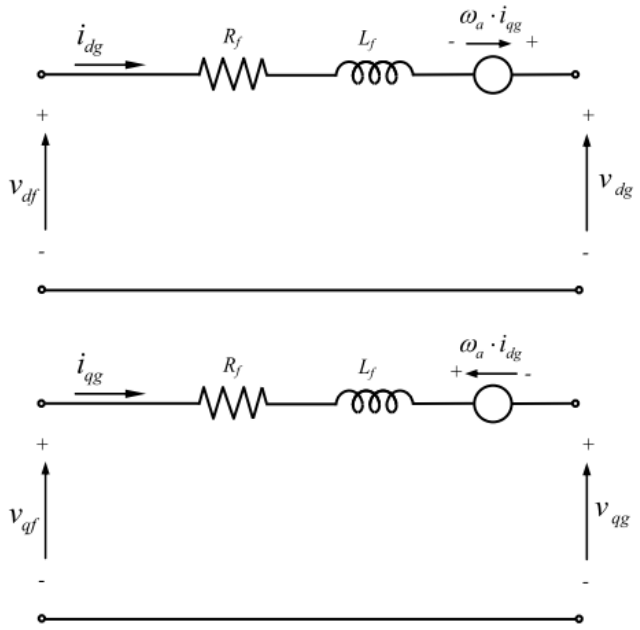

Figure 3.14: Grid side system's equivalent circuit in the dq reference frame [18]

What is key to perform the transformation in a suitable way, is to choose a rotational speed such that the system maintain simple equations or simplify even more. Generally, the

best way is to impose the synchronous rotational angular speed equal to the grid one, resulting in:

$$\omega_a = \omega_s \;\Rightarrow\; \theta = \omega_a t \;\Rightarrow\; \theta_g = \omega_s t \tag{3.25}$$

Consequently, the d-axis is aligned with the grid voltage space vector [18] and the q-axis is equal to 0, consequently, the equations are simplified as:

$$\begin{cases} v_{df} = R_f i_{dg} + L_f \frac{di_{dg}}{dt} + v_{dg} - \omega_a L_f i_{qg} \\ v_{qf} = R_f i_{qg} + L_f \frac{di_{qg}}{dt} + \omega_a L_f i_{dg} \end{cases} \tag{3.26}$$

With this set of equations is possible to define a control system for the grid side converter, as will be shown in the next chapter.

3.5 Power converters for DFIG drive

In order to control the torque, the speed and the power produced by the DFIM, it is necessary to control the voltages and currents of the electrical machine, and in order to this it is necessary some kind of power converter that, given a certain reference for one parameter, is going to modify the voltages in input of the machine (rotor voltages in this case) to reach that specific desired reference.

3.5.1 Architecture and working principle

In the case of DFIM, the converter used is an AC-DC-AC converter that links the rotor windings to the grid, remembering that instead the stator windings are linked directly to the grid. This AC-DC-AC converter is called back-to-back converter (B2B) and it's the combination of two voltage source inverters (VSI) with a capacitor (DC link) between the two converters.

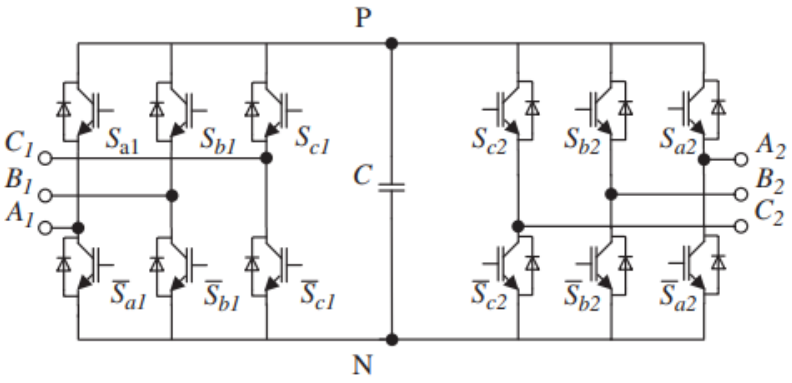

Figure 3.15: Two-level voltage source converters' AC-DC-AC configuration [17]

The two converters can be considered identical for our purpose and composed of six ideal switches for simplicity, but as explained well in [15] and [17] normally in high power converters those are constituted by Insulated Bipolar Transistors (IGBT).
The main idea about the six-switch converter is that is able to generate a sinusoidal output voltage which amplitude, phase and frequency is regulated through a precise series of impulses

Figure 3.16: Example of commercially available back-to-back converter [17]

that turns ON or OFF the state of the switch. This series of impulses is with a fixed frequency but variable width, this is commonly known as Pulse Width Modulation (PWM).
The pulses are created by the comparison of two waves: the modulant, which is responsible for defining the waveform desired in output, and the carrier which is used to define if the PWM signal must be on ON or OFF. An example of the phenomenon can be seen in Figure 3.17.

The most important parameter in the modulation is how much time the signal is ON, defined relatively to the inverse of the switching frequency: this parameter take the name of duty cycle:

$$m = \frac{t_{1,on}}{T_{sw}} \tag{3.27}$$

In a three-phase converter the modulation index are one for each phase, and consequently every phase of the system, relatively to the 0V node can be regulated independently.

$$V_{out} = V_{dc}\frac{t_{1,on}}{T_{sw}} = mV_{dc} \tag{3.28}$$

As can be noticed from (3.29), the voltage output is a fraction of the voltage on the DC side of the converter, that for the case of the B2B converter will be the capacitor voltage on the dc link.

$$\begin{cases} V_{ao} = m_a V_{dc} \\ V_{bo} = m_b V_{dc} \\ V_{co} = m_c V_{dc} \end{cases} \tag{3.29}$$

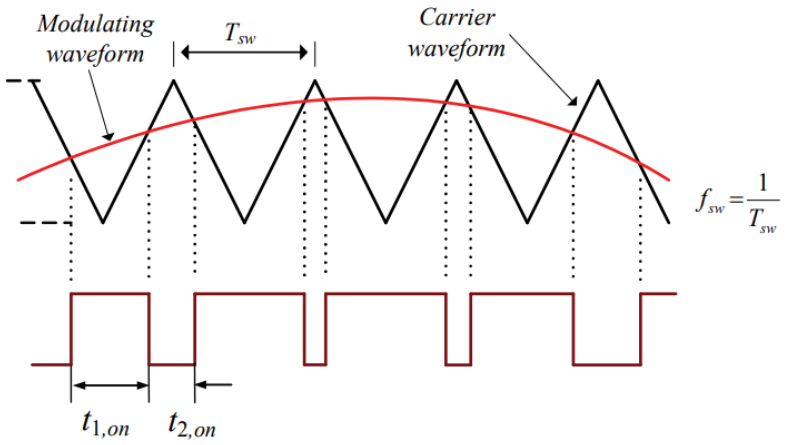

Figure 3.17: Example of carrier-based modulation for PWM signal generation [15]

$$\begin{cases} m_a = \frac{1}{2} + m\sin(\omega t) \\ m_b = \frac{1}{2} + m\sin(\omega t - \frac{2\pi}{3}) \\ m_c = \frac{1}{2} + m\sin(\omega t + \frac{2\pi}{3}) \end{cases} \tag{3.30}$$

So the resultant output voltages for the converter will have the form:

$$\begin{cases} V_{ab} = V_{ao} - V_{bo} = \sqrt{3}m\sin(\omega t - \frac{\pi}{6}) \\ V_{bc} = V_{bo} - V_{co} = \sqrt{3}m\sin(\omega t - \frac{5\pi}{6}) \\ V_{ca} = V_{co} - V_{ao} = \sqrt{3}m\sin(\omega t + \frac{\pi}{2}) \end{cases} \tag{3.31}$$

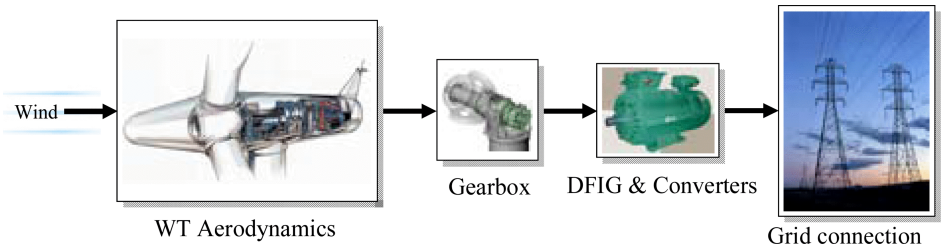

Figure 3.18: Block scheme representing how the system has been implemented [24]

In order to design the electrical system for the wind turbines, it has been chosen, as for the turbine itself, to use a model based design approach, and to implement the system as a series of blocks imported from the Simscape power system library. In this way, the prototyping of the system can be done in a faster way, and major attention and time can be focused later on the control algorithms.
As can be seen from Figure 3.19, the Simulink implementation is very similar to the schemes showed before.

DFIG's Parameter	**Symbol**	**Value**	**Unit measure**
Stator frequency	f	50	[Hz]
Rated stator power	P_s	2e6	[W]
rated rotational speed	n	157,23	[rad/sec]
Rated stator voltage	V_s	690	[V]
Rated stator current	I_s	1760	[A]
Rated torque	T_{em}	12732	[Nm]
pole pairs	p	2	[/]
stator/rotor turns ratio	u	1/3	[/]
rated rotor voltage	V_r	2070	[V]
maximum slip	s_{max}	1/3	[/]
Stator resistance	R_s	2.6e-3	[Ω]
Leakage inductance	L_{si}	0.087e-3	[H]
Magnetizing inductance	L_m	2.5e-3	[H]
Rotor resistance wrt the stator resistance	R_r	2.9e-3	[Ω]
Stator inductance	$L_s = L_m + L_{si}$	0.0026	[H]
Rotor inductance	$L_r = L_m + L_{si}$	0.0026	[H]
DC bus voltage wrt to stator voltage	V_{bus}	1150	[V]
rotor inertia	J	127	[Kg.m^2]
rotor damping (friction factor)	D	1e-3	[N.m.s]
RL Filter's Parameter	**Symbol**	**Value**	**Unit measure**
Grid side filter resistance	R_g	20e-6	[Ω]
Grid side filter inductance	L_g	600e-6	[H]
RSC-GSC's Parameter	**Symbol**	**Value**	**Unit measure**
Snubber resistance	$R_{snubber}$	1e5	[Ω]
Snubber capacitance	$C_{snubber}$	inf	[F]
Internal resistance	V_n	1e-3	[Ω]
Switching frequency	f_{sw}	2e3	[Hz]
DC bus capacitance	C_{bus}	80e-3	[F]
3-Phase Transformer's Parameter	**Symbol**	**Value**	**Unit measure**
Nominal power	V_n	570	[V]
frequency	V_n	570	[V]
Winding 1 voltage	Vy_1	670	[V]
Winding 1 resistance	Ry_1	0	[Ω]
Winding 1 inductance	Ly_1	0	[H]
Winding 2 voltage	Vy_2	670	[V]
Winding 2 resistance	Ry_2	0	[Ω]
Winding 2 inductance	Ly_2	0	[H]
Magnetization resistance	R_{mag}	1.0805e+06	[Ω]
Magnetization inductance	L_{mag}	2866	[H]

Table 3.1: Parameters for the the components of the electrical system modeled in MATLAB/SIMULINK

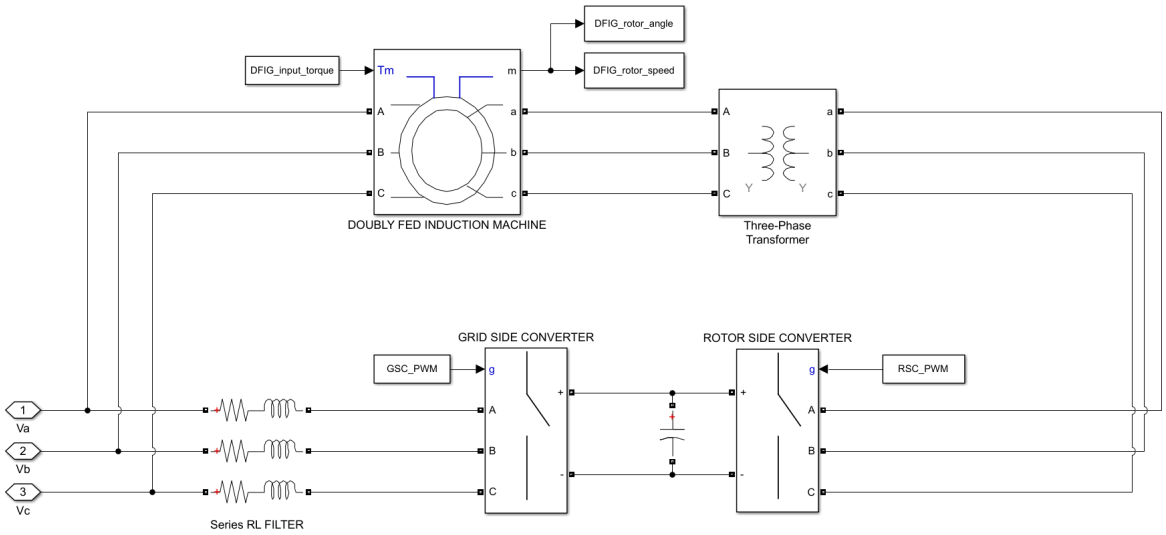

Figure 3.19: DFIG drive implementation on Simulink [MATLAB]

Chapter 4

WIND TURBINE CONTROL

In this chapter, a description of the control block scheme implemented for the back-to-back converter is presented. It is then presented an introduction to the sliding mode control technique, with particular emphasis to the super-twisting sliding mode control, that is the one applied in this project. Finally, the MATLAB/Simulink implementation is presented.

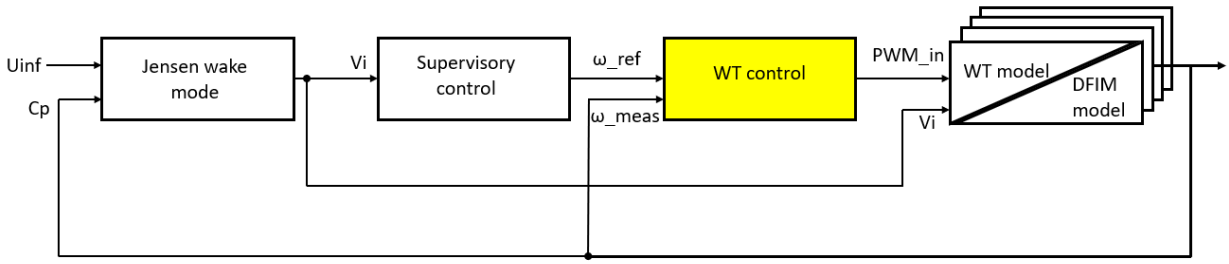

Figure 4.1: Research block scheme: this chapter focuses on the design of the control algorithm for the single WT

4.1 DFIG drive control schemes

In order to produce active power at a desired rotational speed, a control scheme has to be designed, more specifically with the following goals:

1. Maintain a desired voltage on the DC-link in the AC-DC-AC converter
2. Keep the reactive power production as low as possible
3. Tracking a desired rotational speed while the wind impose a torque on the shaft of the generator

In order to achieve this goals, the control schemes must work on both electrical and mechanical parameters, and thanks to the dq reference frame, this is achievable with a double loop control structure. This kind of approach is the nowadays standard for most of the electrical machines available, and here we will focus on the scheme used for the DFIM used in this project.

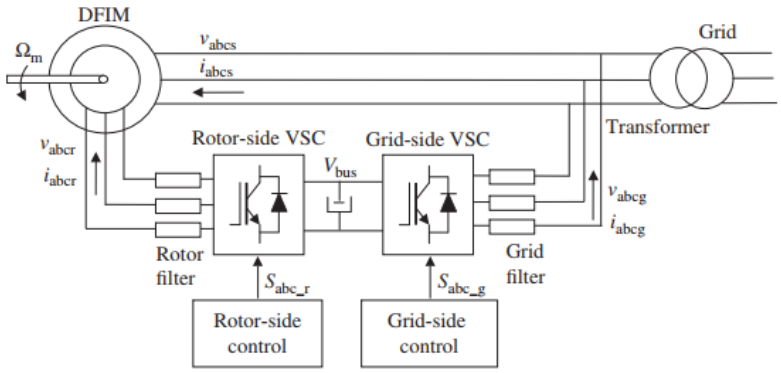

Figure 4.2: Electrical system schematic representation with relative control inputs [14]

4.1.1 Rotor side converter control

The main goal of the RSC is the control of the DFIM itself, that means tracking desired values for speed and currents. The internal loop, as shown in Figure 4.2 is responsible for the tracking of desired values of the rotor currents, which are then responsible for the electromagnetic torque and the reactive power produced by the machine.

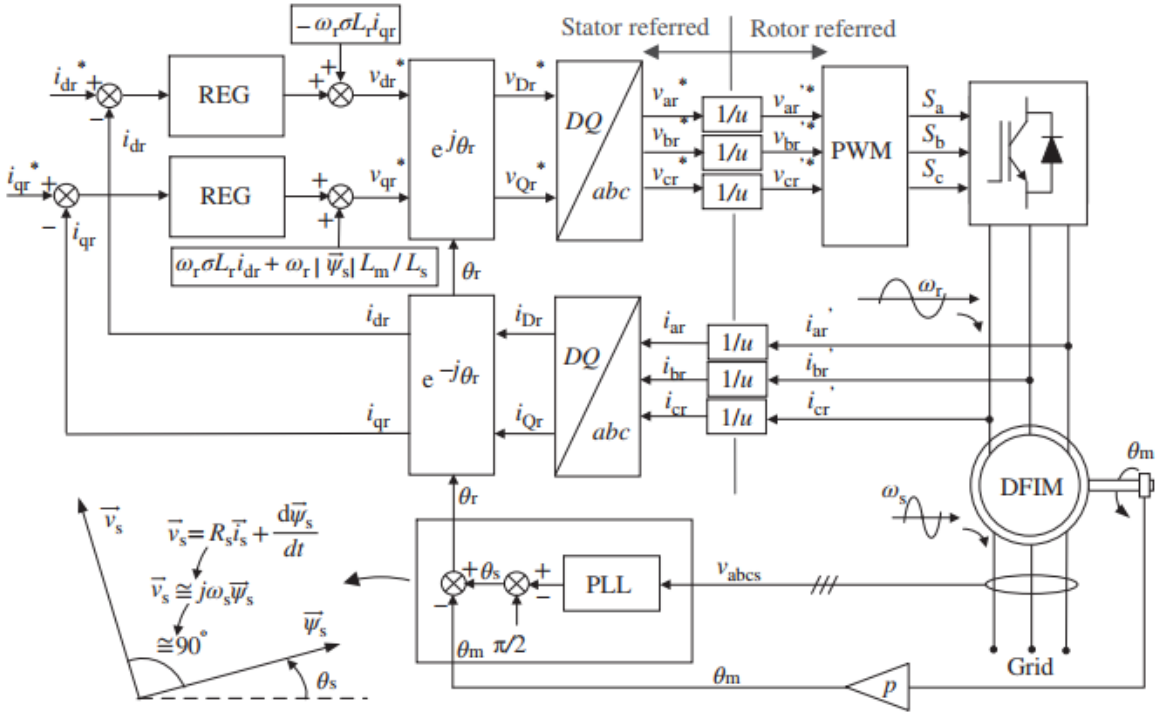

Figure 4.3: Rotor side converter control scheme, including reference transformations [14]

In order to design the vector control law for the current loop, the rotor voltage equation

must be defined, as done in [14]:

$$\begin{cases} v_{dr} = R_r i_{dr} + \sigma L_r \frac{d}{dt} i_{dr} - \omega_r \sigma L_r i_{qr} + \frac{L_m}{L_s} \frac{d}{dt} |\Psi_s| \\ v_{qr} = R_r i_{qr} + \sigma L_r \frac{d}{dt} i_{qr} + \omega_r \sigma L_r i_{dr} + \omega_r \frac{L_m}{L_s} \frac{d}{dt} |\Psi_s| \end{cases} \tag{4.1}$$

For the control design and modeling, the resistance of the rotor windings R-r and the relative voltage will be not considered due to its low value. Then the electromagnetic torque is defined:

$$T_{em} = \frac{3}{2} p \frac{L_m}{L_s} (\Psi_{qs} i_{dr} - \Psi_{ds} i_{qr}) \;\Rightarrow\; T_{em} = -\frac{3}{2} p \frac{L_m}{L_s} |\Psi_s| i_{qr} \;\Rightarrow\; T_{em} = K_T i_{qr} \tag{4.2}$$

This equation shows a really important consideration for the control design: due to the fact that the d-axis of the reference frame is aligned with the stator flux, this means that the term including the direct component of the rotor current in equation is equal to 0. As a result, the electromagnetic torque depends exclusively on the q-component of the rotor current.
This result is very important because the control scheme will be much simpler, and the speed loop, which will be explained later on, will be external on the q-current loop and indipendente from the d-current one.
A similar observation can be done for the reactive power, as shown in the equation below, it

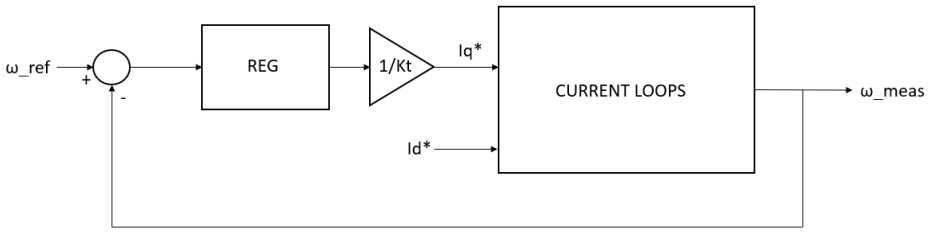

Figure 4.4: Speed control loop's block scheme reprensentation

depends exclusively on the d-component of the rotor current, and so, again, the control loop for the reactive power is external to the d-current one but not linked to the q-current.

$$Q_s = \frac{3}{2}(v_{qs} i_{ds} - v_{ds} i_{qs}) \;\Rightarrow\; Q_s = -\frac{3}{2} \omega_s \frac{L_m}{L_s} |\Psi_s| (i_{dr} - \frac{|\Psi_s|}{L_m}) \;\Rightarrow\; Q_s = K_Q (i_{dr} - \frac{|\Psi_s|}{L_m}) \tag{4.3}$$

$$|\Psi_s| = \Psi_{ds} = L_s i_{ds} + L_m i_{dr} \qquad \Psi_{qs} = 0 = L_s i_{qs} + L_m i_{qr} \tag{4.4}$$

An important mention goes also to the estimation of theta, necessary to compute the reference trasnformations. Traditionally, this is done done with a specifically design controller called Phase Locked Loop (PLL), that can be implemented as a PID controller or other techniques.
In this research, the PLL has been simplified with a trigonometric function that takes in input the stator voltage in the alpha/beta domain:

$$\theta_r = atan2(v_\alpha, v_\beta) - \frac{\pi}{2} - p\theta_m \tag{4.5}$$

4.1.2 Grid side converter control

With a similar approach to one used for the rotor side converter, due to the fact that thanks to the dq reference frame, the active and reactive power are separated, it is possible to define two independent control loops for active and reactive power.

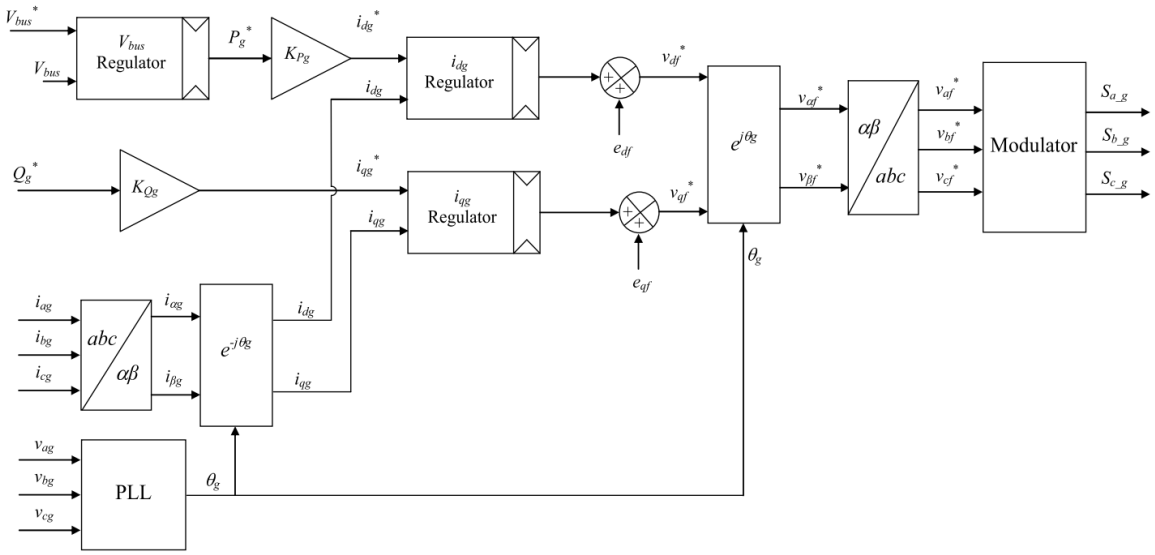

Figure 4.5: Grid side converter control scheme, including reference transformations [18]

As shown in Figure 4.5, the d-axis control voltage is function of the d-axis current, which is directly correlated to the active power by means of a constant gain. The outer loop regulator, that control the DC-bus voltage of the back to back converter, gives in output in fact a reference value for the active power necessary to flow, this demonstrates how important is to control the DC-bus voltage: the power flowing through the converter is function of the voltage on the DC-bus.
The q-axis control instead, is used to control reactive power flow through the converter, and again, the power is directly connected with the current through a constant gain.

$$\begin{cases} K_{Pg} = \frac{1}{\frac{3}{2}v_{dg}} \\ K_{Qg} = \frac{1}{-\frac{3}{2}v_{dg}} = -K_{Pg} \end{cases} \tag{4.6}$$

It is also important to mention that to perform best the control loops, coupling terms for both the equations are defined and added to the output of the current regulators:

$$\begin{cases} e_{df} = -\omega_s L_f i_{qg} \\ e_{qf} = \omega_s L_f i_{dg} \end{cases} \tag{4.7}$$

Finally, as for the rotor side converter, an estimation of the theta for the reference transformation is defined as:

$$\theta_r = atan2(v_\alpha, v_\beta) \tag{4.8}$$

4.2 Control algorithms

Traditionally, industries' approach to control algorithms is based on the well-founded PI control technique, which is simple and intuitive to understand from a physical point of view and generally simple to tune and design. Unfortunately PI control presents certain limits in terms of

1. robustness to model uncertainty and disturbances
2. risk of saturation due to the integral component, and consequent problems of windup

In order to design a better control for the system, a super-twisting sliding mode control strategy is proposed, with a simplified description of the sliding theory and the definition of the control algorithm for then moving forward to its application in the DFIM control scheme.

4.2.1 Elementary introduction to sliding mode control

As well described in [21], [22] and [23] sliding mode control is a non-linear control technique characterized by accuracy and robustness to parameter uncertainties and disturbances. Another major point is the easiness of the tuning of the parameters.
The general approach to it is characterized by two major points:

1. definition of the sliding surface, which if done correctly can modify the dynamic behaviour of the system
2. design of the control law, which goal is to make the state reach the surface and staying close to it.

For simplification, we consider a SISO non linear system:

$$\dot{x} = f(x,t) + g(x,t)u \tag{4.9}$$

$$y = h(x,t) \tag{4.10}$$

where the state x is measured and no observers are needed.
The goal of the control system is the tracking of a desired value Y, which means, that after a finite period of time, the tracking error e = Y - y, where y is the measured value has to converge to 0.
The definition of the sliding surface can be done in various ways, depending on the complexity of the system and on the desired behaviour, but normally, the sliding function can be defined as linear combination of the tracking error and its derivatives:

$$\sigma = \sigma(e, \dot{e}, e^{(2)}, \ldots, e^{(k)}) \tag{4.11}$$

For the purpose of this research, the sliding function has been defined simply as the tracking error itself:

$$\sigma = e = y_{ref} - y_{meas} \tag{4.12}$$

By forcing this function to 0, the sliding surface is defined:

$$\sigma = e = y_{ref} - y_{meas} = 0 \tag{4.13}$$

The next step is the definition of a control law, such that the command input u "forces" the system trajectory to move in direction of the sliding surface and to remain in its proximity. In this way we can observe the two main properties of the sliding mode control:

1. attractive, the system moves versus the surface
2. invariant, the system remains on the surface

As explained in [23], a peculiar feature of the sliding mode control techniques, is that to design the control law it is not necessary to have a very precise idea of the plant's model, that can be treated as a kind of black box model.

The most simple form of sliding mode control is the first order sliding mode control, which can be defined as

$$u = -Ksign(\sigma) \tag{4.14}$$

Which basically means that the command input switches between two values with a certain frequency, and the higher the frequency the faster is the convergence to the surface.
Nonetheless, this kind of control technique, suffers from a phenomenon called chattering, that can be seen in Figure 4.6, where the system never converges to the surface, but oscillates around it. This can be acceptable for certain applications such as certain kinds of power converters, but in other applications such as electro-mechanical systems, the chattering generally tends to create various problems such as ripples in speeds or torques.
In order to avoid the chattering phenomenon, an increase in the order of the sliding mode control is a generally effective solution that maintains the robustness features. In this research, more precisely, a particular kind of second order sliding mode control is discussed and applied. Known as the super-twisting sliding mode control, a brief description is presented in the next section.

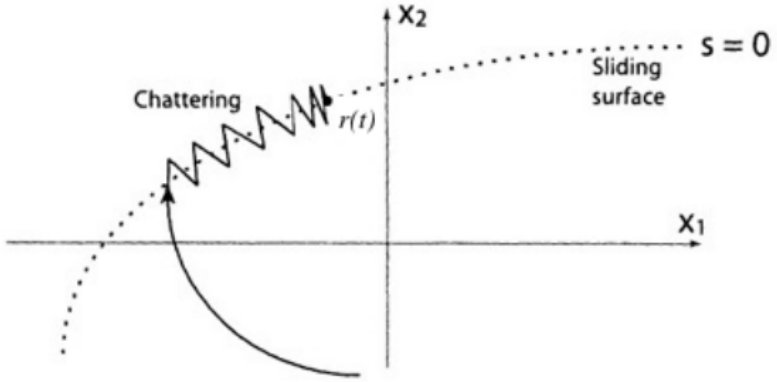

Figure 4.6: Chattering effect of the first order sliding mode control [21]

4.2.2 The super-twisting sliding mode control

As well described in [22], the super-twisting sliding mode control, is a second order sliding mode control technique, characterized by the fact that it doesn't require any measure/observation of the derivative of the sliding surface (that in our case, we remember, is equal to the tracking error itself). This means that, even with a simple algorithm, it is possible to have a robust algorithm:

$$u = -A_1|\sigma|^{\frac{1}{2}} sign(\sigma) + u_1 \tag{4.15}$$

$$\dot{u_1} = -A_2 sign(\sigma) \tag{4.16}$$

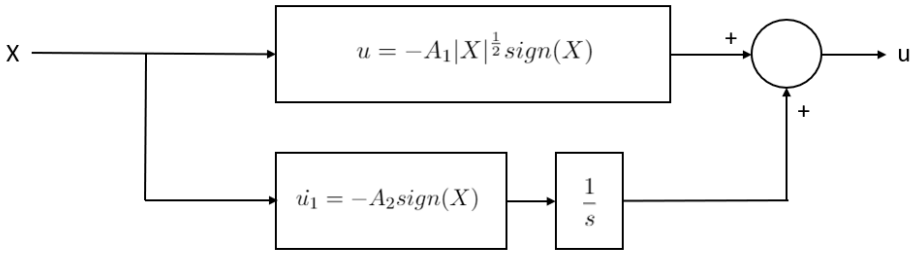

Figure 4.7: Super-twisting sliding mode control's block scheme
where X is the tracking error/sliding surface

Another advantage of this technique is that the tuning of the parameters is limited to only two parameters, and by gradually increasing the values, by means of trial and error, is quite suitable for industrial applications [23].

4.3 DFIM super-twisting control's application

4.3.1 Rotor side converter control application

As well explained in [24], sliding mode control is demonstrated to be very effective for WT systems, due to its robustness to uncertainties and to the torque's oscillation's smoothing. Nonetheless, a first order sliding mode control can still problems related to the chattering effect, that in terms of torque, means ripple and consequent mechanical stress.
In order to avoid this problems, a second order sliding mode control like the super-twisting one, with all the advantages described before. For the purpose of this paper, the sliding surface S, has been defined in a simpler way considering exclusively the tracking error of the desired variables. This approach, however, is not the most rigorous one, and without the relative constraints due to the surface, the choose of the parameters for achieving the desired performance requires many trial and errors. A formulation of the control laws for the RSC is now presented.
As can be seen in Figure 4.4, as explained before, the outer loop of the speed control, is external only to the q-component of the rotor current:

$$\begin{cases} u_\omega = -A_{w1}|\omega_{meas} - \omega_{ref}|^{\frac{1}{2}} sign(\omega_{meas} - \omega_{ref}) + u_1 \\ \dot{u_1} = -A_{w2} sign(\omega_{meas} - \omega_{ref}) \end{cases} \tag{4.17}$$

But the output of the speed controller by itself, is by definition the electromagnetic torque, that mechanically opposes the mechanical torque in input coming from the wind turbine shaft.Remembering that, the current reference value for the inner control loop:

$$I_{qr-ref} = (-u_\omega \frac{2}{3pF_s \frac{Lm}{Ls}}) = u_\omega K_T^{-1} \tag{4.18}$$

The currents regulators implement the same control algorithm:

$$\begin{cases} u_{I_{dr}} = -A_{1dr}|I_{dr-meas} - I_{dr-ref}|^{\frac{1}{2}} sign(I_{dr-meas} - I_{dr-ref}) + u_1 \\ \dot{u_1} = -A_{2dr} sign(I_{dr-meas} - I_{dr-ref}) \end{cases} \tag{4.19}$$

$$\begin{cases} u_{I_{qr}} = -A_{1qr}|I_{qr-meas} - I_{qr-ref}|^{\frac{1}{2}} sign(I_{qr-meas} - I_{qr-ref}) + u_1 \\ \dot{u_1} = -A_{2qr} sign(I_{qr-meas} - I_{qr-ref}) \end{cases} \tag{4.20}$$

And the final values for the command inputs are defined following the voltage laws described before, remembering that the voltage drop on the resistance has been neglected:

$$v_{dr-cmd} = u_{I_{d-r}} - (2\pi f - p\omega_m) L_r I_{qr-1} \tag{4.21}$$

$$v_{qr-cmd} = u_{I_{q-r}} + (2\pi f - p\omega_m)\sigma L_r I_{dr-meas} + (2\pi f - p\omega_m)\frac{L_m}{L_s} F_s \tag{4.22}$$

4.3.2 Grid side converter control application

Following an analog path, also for the GSC, all the regulators have been implemented using the super-twisting algorithm:

$$\begin{cases} u_V = -A_{1V}|V_{dc-meas} - V_{dc-ref}|^{\frac{1}{2}} sign(V_{dc-meas} - V_{dc-ref}) + u_1 \\ \dot{u_1} = -A_{2V} sign(V_{dc-meas} - V_{dc-ref}) \end{cases} \tag{4.23}$$

But the output of this algorithm, in terms of physical characteristic, is a power. Following the equations described before:

$$I_{dg-ref} = u_V \frac{2}{3V_s\sqrt{\frac{2}{3}}} \tag{4.24}$$

$$\begin{cases} u_{I_{dg}} = -A_{1dg}|I_{dg-meas} - I_{dg-ref}|^{\frac{1}{2}} sign(I_{dg-meas} - I_{dg-ref}) + u_1 \\ \dot{u_1} = -A_{2dg} sign(I_{dg-meas} - I_{dg-ref}) \end{cases} \tag{4.25}$$

$$\begin{cases} u_{I_{qg}} = -A_{1qg}|I_{qg-meas} - I_{qg-ref}|^{\frac{1}{2}} sign(I_{qg-meas} - I_{qg-ref}) + u_1 \\ \dot{u_1} = -A_{2qg} sign(I_{qg-meas} - I_{qg-ref}) \end{cases} \tag{4.26}$$

As for the rotor side converter, the voltage drop on the filter resistance has been neglected, and to the command input is added the coupling terms of (4.7):

$$v_{dg-cmd} = u_{I_{dg}} - 2\pi f L_g I_{qg} \tag{4.27}$$

$$v_{qg-cmd} = u_{I_{q-g}} + 2\pi f L_g I_{dg} \tag{4.28}$$

Solver's type	Fixed step
Solver	ode4 (Runge-Kutta)
Fixed step size	0.0005 sec.
Parameter	Value
A_{w1}	7000
A_{w2}	3000
A_{1qr}	4000
A_{2qr}	20000
A_{1dr}	4000
A_{2dr}	20000
A_{1V}	-70000
A_{2V}	-700000
A_{1qg}	10000
A_{2qg}	10000
A_{1dg}	4000
A_{2dg}	45000

Table 4.1: Super-twisting sliding mode control parameters

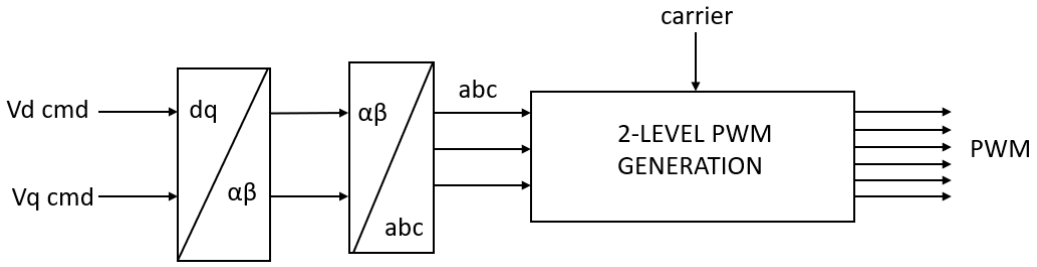

Figure 4.8: Conversion steps of the command output from the control to the converter

The implementation of the control algorithm, by means of MATLAB/Simulink, comprehended the design of a block scheme, following the ones present in Figure 4.3 4.4 and 4.5. An important mention is necessary to do for the conversion of the command inputs: the values in the dq domain has to be converted again in the three-phase domain, then they need to be normalized to be compared with the carrier for the pwm generation. The last passage is done automatically by a block function from the MATLAB/Simulink libraries, which generates internally the carrier signal.

Chapter 5

WIND FARM OPTIMIZATION ALGORITHM

5.1 Introduction

In this chapter, a presentation of the supervisor control for the wind farm is presented.In this case, instead of applying the more common Maximum Power Point Tracking (MPPT), a polynomial optimization problem for the best trade-off between power produced and, damage and fatigue, is presented. This optimization problem consider also the partial wake model described in chapter 2.

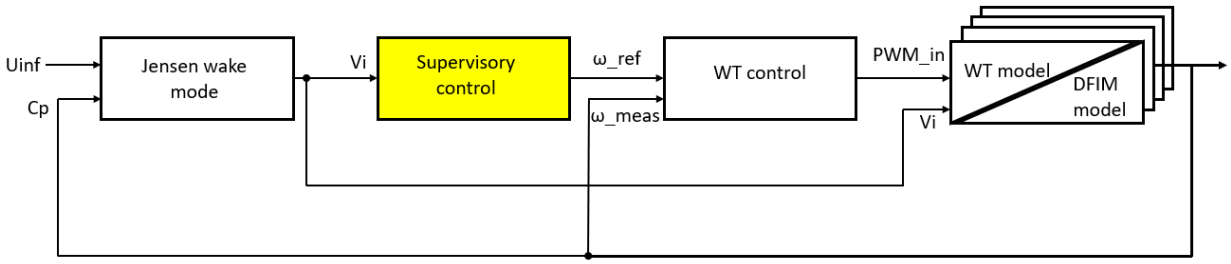

Figure 5.1: Research block scheme: this chapter focuses on the design of the supervisory control algorithm for the wind farm

5.2 Problem formulation

Now that the modeling and control of the single turbine has been completed, it's possible to define the supervisory control for the wind farm, which is the responsible for the computation of the reference rotational speed for the DFIMs of the turbines.
The optimization problem presented here has been implemented originally in [20], where the author were considering a linear array of wind turbines, which characteristics were described by means of the actuator disk model:

$$a = \frac{U_\infty - U_{R,i}}{U_\infty}$$

The definitions for power and thrust for the j-th turbine are described in the same way:

$$C_{P,j} = 4a_j(1-a_j)^2 \Rightarrow P_j = \frac{1}{2}\rho A C_p v_j^3 \Rightarrow P_j = ca_j(1-a)^2 v_j^3 = f(a_i, U_\infty)_j \tag{5.1}$$

$$C_{T,j} = 4a_j(1-a_j) \Rightarrow T_j = \frac{1}{2}\rho A C_T v_j^2 \Rightarrow T_j = ca_j(1-a_j) v_j^2 = f(a_i, U_\infty) \tag{5.2}$$

where c = 2rhoA and the only variables are Uinf and ai

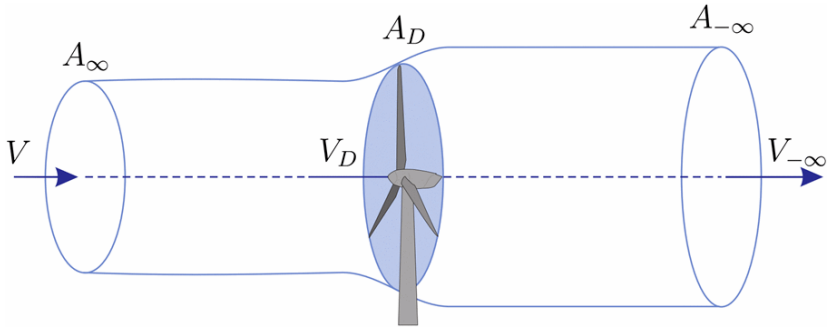

Figure 5.2: Actuator disk model representation [25]

But the application of this linear array's description limits the possible studies to other kinds of layout: a description of the layout of this research, a diamond shape, for example, could lack of details for applying correctly the optimization algorithm. The idea in this research is to apply the same kind of model but where the wind speeds vj are defined by means of the already described Jensen wake model, which consider also the effect of partial waking:

$$v_j(x_{ij}) = U_\infty \left[1 - \sum \left(1 - \sqrt{1-C_T}\right)\left(\frac{r_0}{r_i(x_{ij})}\right)^2 \frac{A_{shadow,i}}{A_0}\right] = f(a_i, U_\infty) \tag{5.3}$$

The estimation of fatigue damage can be done in various ways, depending on the level of details required for the application. As in [20], it is considered that the main driver of fatigue damage on the turbine is caused by the turbulence of the input air, which is enhanced by the fact that the WTs are subject to wake meandering. A simple definition of the turbulence intensity I can be done considering it as the ratio between the standard deviation of the wind speed and mean value:

$$I_i = \frac{\sigma_{v,i}}{v_{0,i}} \tag{5.4}$$

The turbulence effect cannot be described by means of the actuator disk model in its standard form due to the many ideal hypothesis assumed. The turbulence effect uses an augmentation of the thrust coefficient [20], described as a polynomial. The formula describing the fatigue damage becomes:

$$\Upsilon_i = c v_i^2 I^2 (z_2 a_i^2 + z_1 a_i + z0) = f(a_i, U_\infty) \tag{5.5}$$

5.3 Optimization problem

The supervisory control algorithm designed in this research can be divided in two main parts:

1. The optimal value computation, in which we find the optimal solution considering power produced, fatigue and damages
2. The optimal value conversion, in which the output of the previous part, is converted into a value applicable as reference value for the control loop of the single wind turbines

After defining power, damages and fatigue for the single turbines, the cost functionals for the entire wind farm are simply defined as the sum of the the single turbines' descriptions. So the total power extraction:

$$J_P(a, U_\infty) = \sum_{j=1}^{N} P_i(a_i, U_\infty) \tag{5.6}$$

The total extreme loads on the turbines' towers:

$$J_f(a, U_\infty) = \sum_{j=1}^{N} T_i(a_i, U_\infty) \tag{5.7}$$

And the total fatigue damage:

$$J_d(a, U_\infty) = \sum_{j=1}^{N} \Upsilon_i(a_i, U_\infty) \tag{5.8}$$

The major point of the cost functionals is that all of the three are function only of the input wind speed, which is known from the Jensen wake model, and of the axial induction factors, that is only unknown variable of this problem. It's necessary now to define a cost function and the constraints for the problem, but due to the fact that maximum values for fatigue and loads are unknown due to the simple model of the wind turbines, the cost functionals of damage and extreme loads cannot be inserted as constraints. A different approach as chosen in [20], is to define a unique cost function with both the power, which goal is to maximize, and the damages, which goal is to be decreased:

$$J(a, U_\infty) = J_P(a, U_\infty) - \zeta J_f(a, U_\infty) - \lambda J_d(a, U_\infty) \tag{5.9}$$

So the final result is a non-linear optimization problem, more precisely a polynomial optimization problem defined in a, without constraints except for the lower and upper bound of a, which is given by Betz limit, already described in chapter 2. The weights zeta and lambda can be tuned for the desired level of caution and power extraction desired for the wind farm. Particular attention can go the condition when zeta = lambda = 0, for which the optimization problem became the same of the Maximum Power Point Tracking, where the target axial induction factor automatically became 0.33, which corresponds to the tracking of the maximum power coefficient Cp, disregarding of the thrust on the turbines or the fatigue damages.

$$max(a \in A): \;\; J(a, U_\infty) = J_P - \zeta J_f - \lambda J_d \;\; s.t. \, 0 < a_i < \frac{1}{3} \;\; (Betz's\, limit) \tag{5.10}$$

The output of this optimization problem, is a vector containing the values, between 0 and 0.33 of the desired axial induction factors for all the turbines in the wind farm.

After obtaining the optimal values for the turbines, it is necessary to convert them into a speed reference for the DFIM of the turbines. Due to the fact that the axial induction factors are defined in function of the wind speed in output of the turbines, a value that is not measurable (assumption for this research), it is necessary to compute another step for transforming the reference.
As known from the actuator disc model, the power coefficient, is a function of the axial induction factor, and this relation is still valid for the optimal value in output of the previous algorithm.

$$C_{P,j} = 4a_j(1 - a_j)^2$$

But it is also known, by the aerodynamics and the structure of the wind turbine, that the power coefficient is also defined from the pitch angle (assumed constant in this research) and the tip-speed ratio:

$$\begin{cases} C_{P,j}(\lambda, \beta) = 0.22 \left(\frac{116}{\kappa_i} - 0.4\beta - 5 \right) e^{\frac{-12.5}{\kappa_i}} \\ \frac{1}{\kappa_i} = \frac{1}{\lambda + 0.08\beta} - \frac{0.035}{\beta^3 + 1} \end{cases}$$

But due to the fact that this relation is highly non-linear, before proceeding, a polynomial approximation has been made:

$$C_{P,j}(\lambda, \beta) \; = \; C_{P,j}(\lambda) = -0.0022\lambda^3 + 0.0218\lambda^2 + 0.0267\lambda - 0.0437 \tag{5.11}$$

These two relations describing the axial induction factor can be equalized, where the only unknown parameter of the system is the tip-speed ratio. In order to find the value of lambda that equalize the two equation, another polynomial optimization problem can be defined:

$$min(\lambda) \; s.t. \; C_{P,j}(\lambda, \beta) \; = \; C_{P,j}(a) \tag{5.12}$$

The tip-speed ratio in output, represents the optimal target value for the WTs. It is also known that the tip-speed ratio is function of the rotational speed of the shaft, that through the gear ratio N and a proportional constant, representing the un-modeled dynamics of the system, the final speed reference value for the DFIM is defined as:

$$\lambda = \frac{\omega R}{V} \; \Rightarrow \; \omega_{opt} = \frac{\lambda_{opt}\omega}{R} \tag{5.13}$$

$$\omega_{ref} = K_{prop} N \omega_{opt} \tag{5.14}$$

For both the polynomial optimization problems, after the testing of various algorithms, it has been chosen to solve them by means of the interior point method algorithm, described in the next section.

5.4 Interior point method algorithm

The interior point method is an algorithm able to solve non-linear (and linear) convex optimization problems. Its main characteristic is that the optimal solution is taken from the

inside of the feasible set (from where takes its name). This algorithm is well explained in [26].

Supposing to have a non-linear optimization problem:

$$min(x): \ f(x), \ s.t. \, h(x) \ = 0 \ and \ g(x) \leq 0 \tag{5.15}$$

An approximation of the problem can be defined through the definition of a barrier function, where the non equality constraints are substituted with a logarithmic barrier function:

$$min(x, s): \ f(x) - \mu \sum_{j=1} ln(s_i) \ \ s.t. \ h(x) = 0 \ and \ g(x) + s = 0 \tag{5.16}$$

where s is the defined as the vector of slack variables where there a slack variable s-i for each non-equality constraint. The term nu is a parameter describing how rapidly the function converges to the barrier. Now the new approximated problem, containing only equality constraints, is easier to solve. This can be done by means of a Newton step or with conjugate gradient step.
In general, the algorithm attempts to apply the Newton step firstly, and at each iteration, the algorithm decreases a merit function [26]:

$$f_\mu(x, s) + \nu \parallel (h(x), g(x) + s) \parallel \tag{5.17}$$

The details about the new Newton step and conjugate gradient techniques are not explained in this elaborate, more information can be found in [26] and [27].

The implementation of both the optimization algorithms has been done by means of the fmincon function of the Optimization toolbox of MATLAB [26]. The system has been implemented in two atomic subsystem in such a way that instead of calling the command at every time step (0.0005 sec), the command in called approximately every 20 seconds. In such way, the DFIG system and the super-twisting sliding mode control can operate to reach the reference values in the proper timing and, of course saving computational power.
The system implement also slew rate limits and saturation blocks in order to avoid step responses, that for this kind of electrical systems, characterized by great values of electrical power (2MW) can risk to reach excessively high values of currents, way over the nominal value.

Chapter 6

RESULTS

In this chapter, the results from the simulations of all the subsystems, performed with MATLAB/Simulink, are presented. The executed simulation include a unique Simulink file with a sampling time of 0.0005 seconds, for a total time of 300 seconds. The first transitory effects are neglected and the focus is on the steady state behaviour of the system, which start from around t = 100 seconds.

6.1 Jensen wake model

As can be seen from Figure 6.1, the wind speed for the turbines 2 and 3 are affected from a small speed deficit due to the proximity to the boundaries of the wake of turbine 1. While instead turbine 4 shows a significant amount of reduction in the input wind speed due to the fact that enters totally in the wake of turbine 1, and partially in turbine 2 and 3.

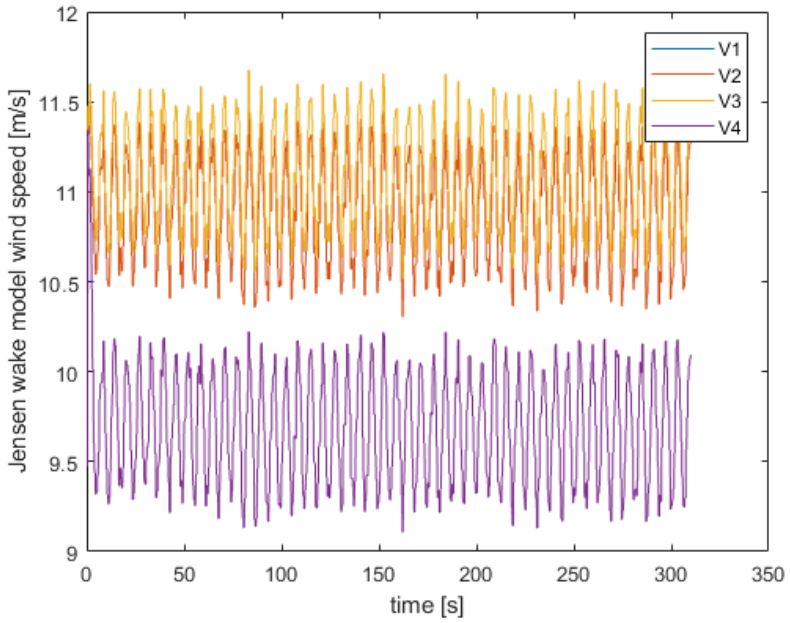

Figure 6.1: Wind speed estimations from the Jensen wake model

6.2 Wind turbine model

In figure 6.3 and Figure 6.4, how the output mechanical torque of a turbine maintains a behaviour similar to the one of the input speed is shown. In this case, a small sinusoidal behaviour is observed.
While in figure 6.2, how the power coefficient of the turbines behaves during the simulation is shown. As expected, the power coefficient is lower than the maximum value of 16/27 due to the fact that the axial induction factor is lower than the 0.33 given by Betz limit. Moreover, the purpose of this application is not to find the MPPT point, but a better trade off for the wind farm system. So this result demonstrates how the system is not forcing itself to the maximum power extraction possible but instead to a lower value in order to reduce mechanical stress, as shown later on.

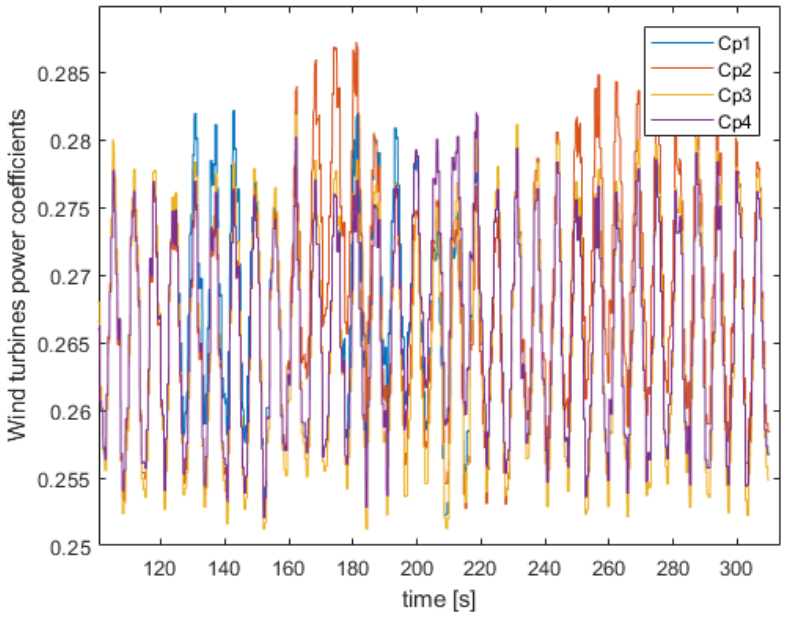

Figure 6.2: Power coefficient measurements for WT 1

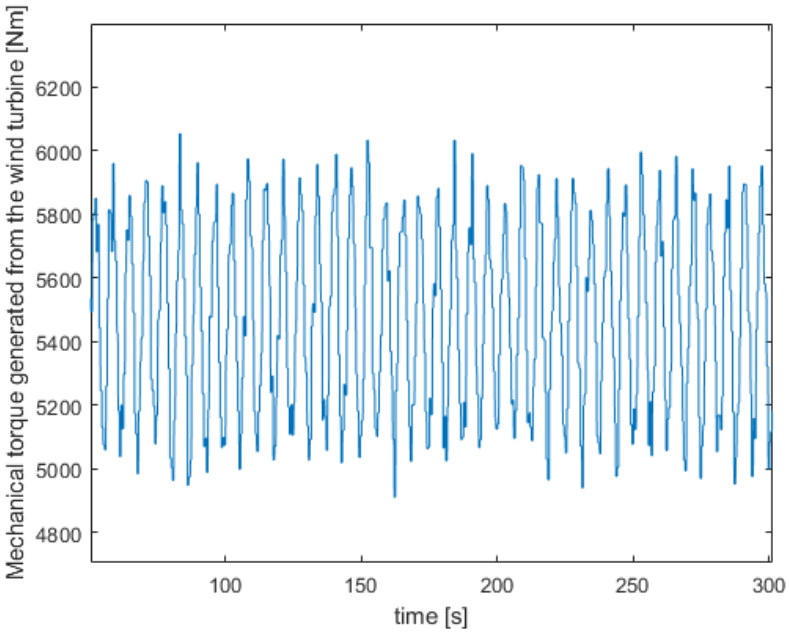

Figure 6.3: Detail of the torque measurements for WT 1

6.3 Doubly fed induction generator model

As shown in Figure 6.5, the voltage of the stator, that we remember is equal to the grid voltage due to the direct linking between them, is not affected by the power generation of the system, and keeps a perfectly balanced 3-phase sinusoidal behaviour.

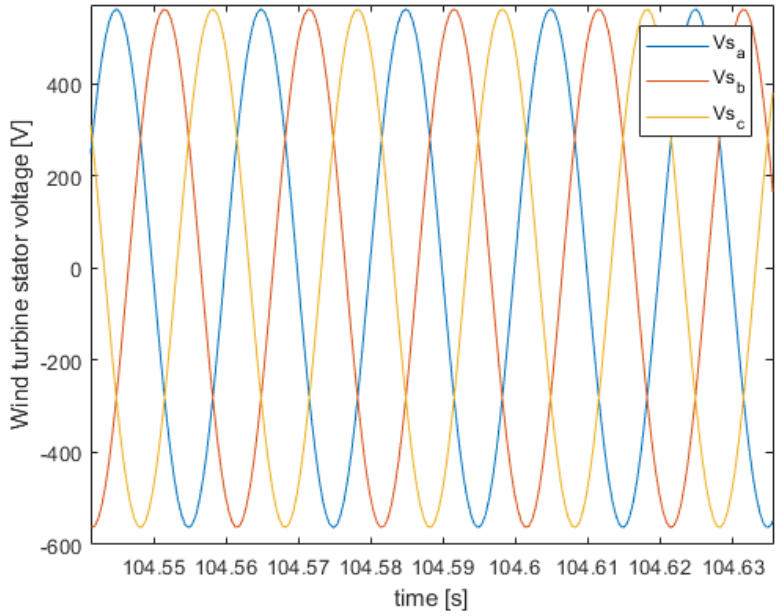

Figure 6.4: Stator voltage measurement

The stator current, as shown in Figure 6.6, maintains a sinusoidal behaviour and the peak values remain under the nominal current of the machine.

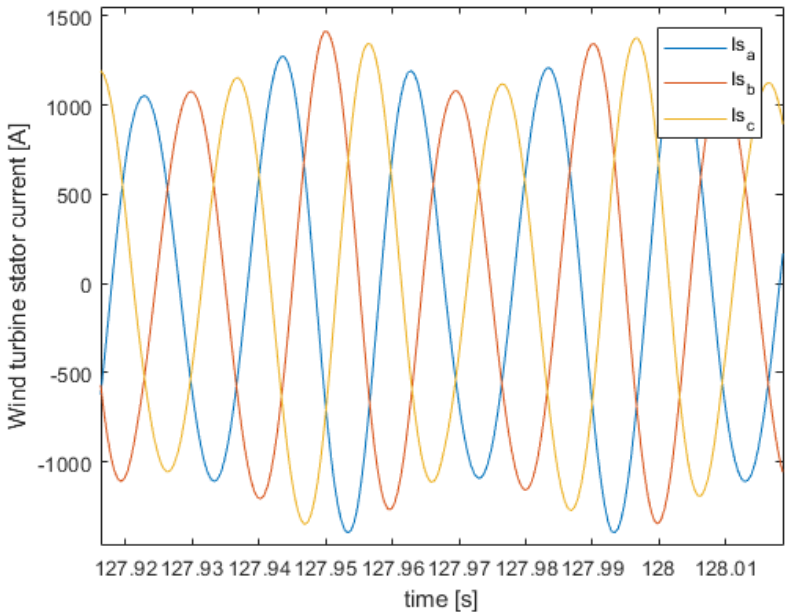

Figure 6.5: Stator current measurement

While the rotor current, as can be seen in Figure 6.6 and 6.7, behaves in a quasi-sinusoidal behaviour. This is due to the 2-level voltage converter topology, the limited switching frequency, and the simplified phase locked loop implementation. Also, the "quality" of the waveform depends also on the rotational speed of the machine. In fact, in Figure 6.8, it can be observed that the frequency of the rotor current has a drop because the rotational speed in that moment was very close to the stator rotating magnetic field's one.

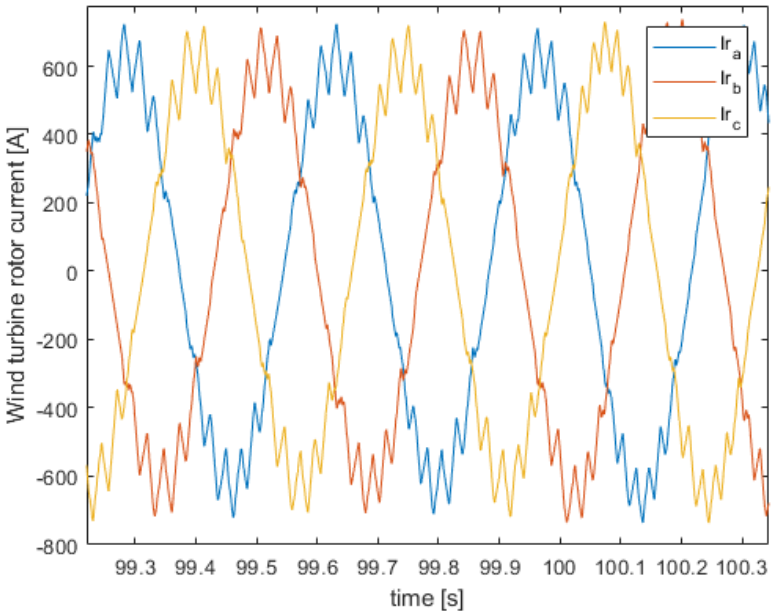

Figure 6.6: Rotor current measurement

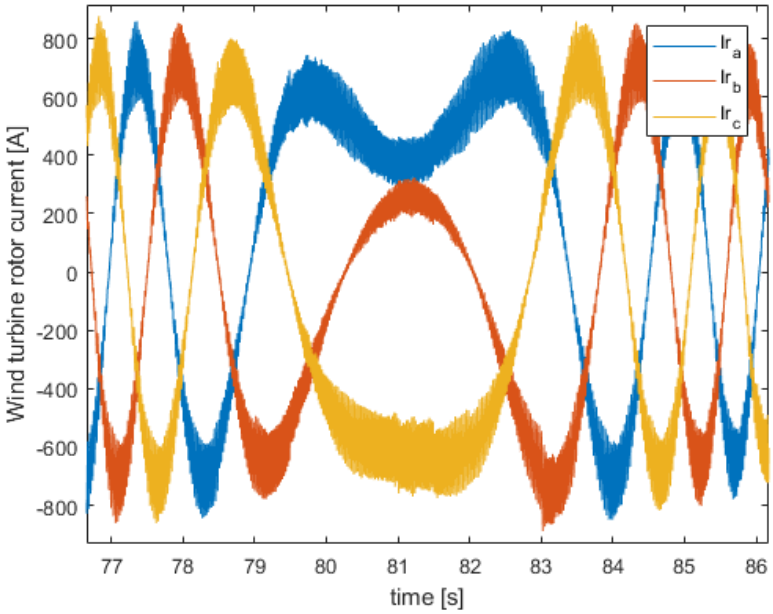

Figure 6.7: Rotor current measurement in proximity of the synchronous speed

6.4 Super-twisting sliding mode control

As can be seen from Figure 6.8, the tracking of the reference speed targets from all the turbines of the wind farm is obtained with good results. It can be seen from Figure 6.14, the

chattering effect given by the switching activity around the reference value. Nonetheless, for such industrial applications, an oscillation of 0.03 rad/sec can be considered acceptable.

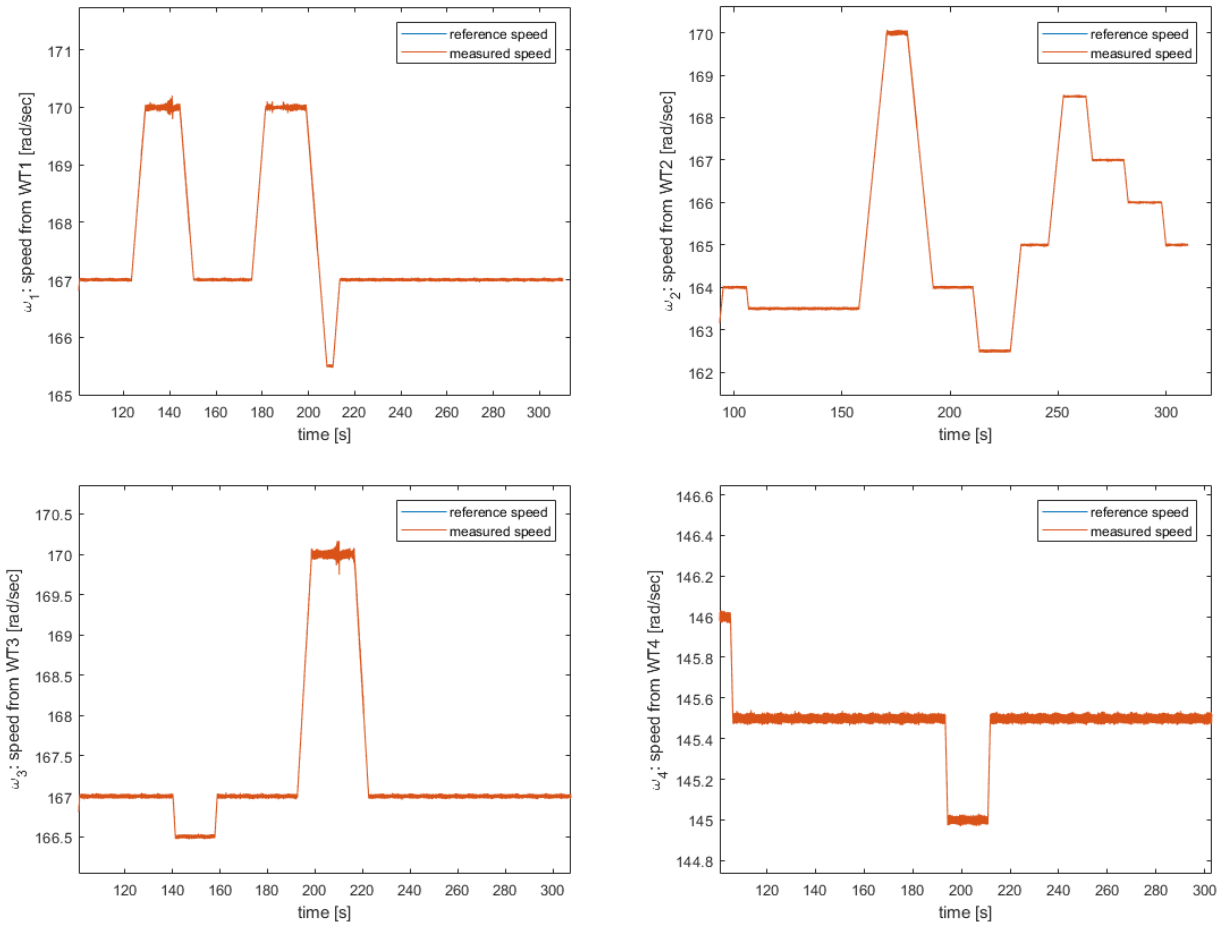

Figure 6.8: Rotational speed measurement

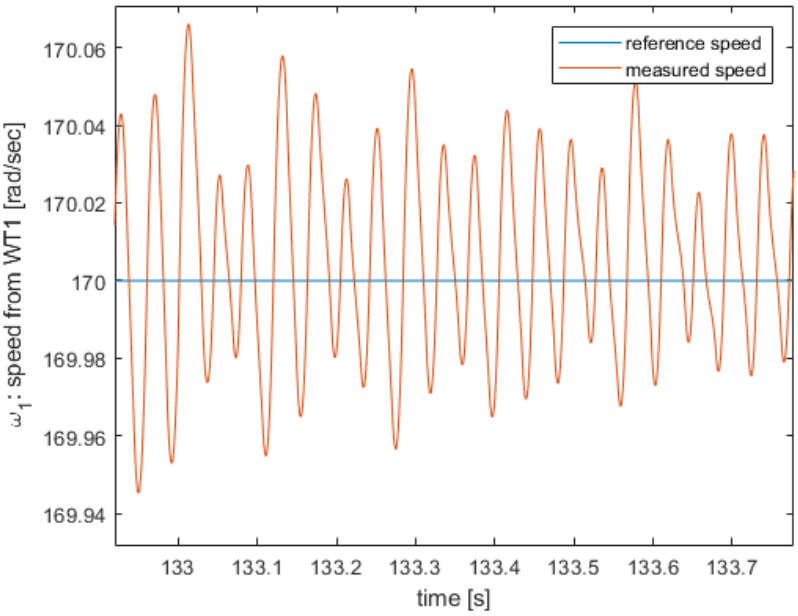

Figure 6.9: Chattering effect of the speed tracking for WT1

In Figure 6.10 instead, it can be seen how the DC Voltage tracking problem presents very high oscillations due to the chattering effect:

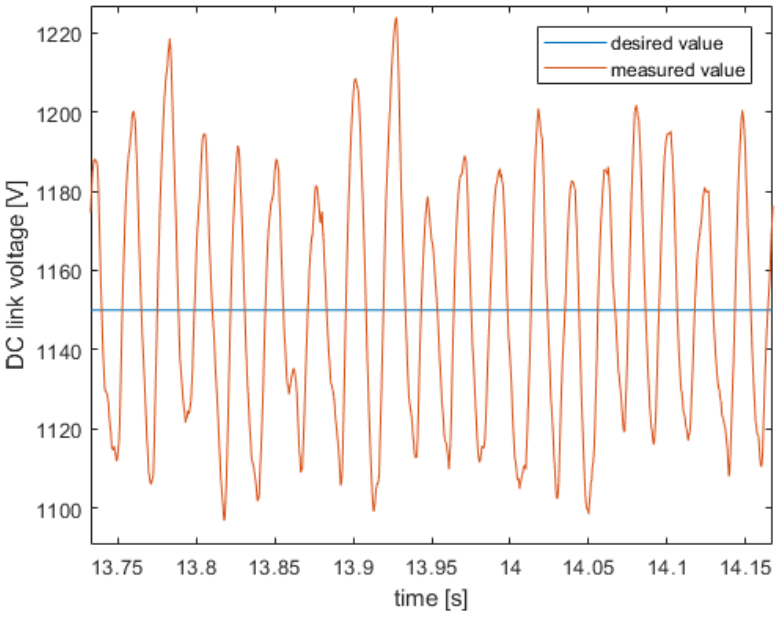

Figure 6.10: Total mechanical power captured by the wind farm

6.5 Wind farm optimization algorithm

As in Figure 6.11, Figure 6.12 and Figure 6.13, the captured power from the wind farm is less compared with maximum power point tracking algorithm (MPPT), but also as the loads on the tower and the fatigue damages are slightly reduced.

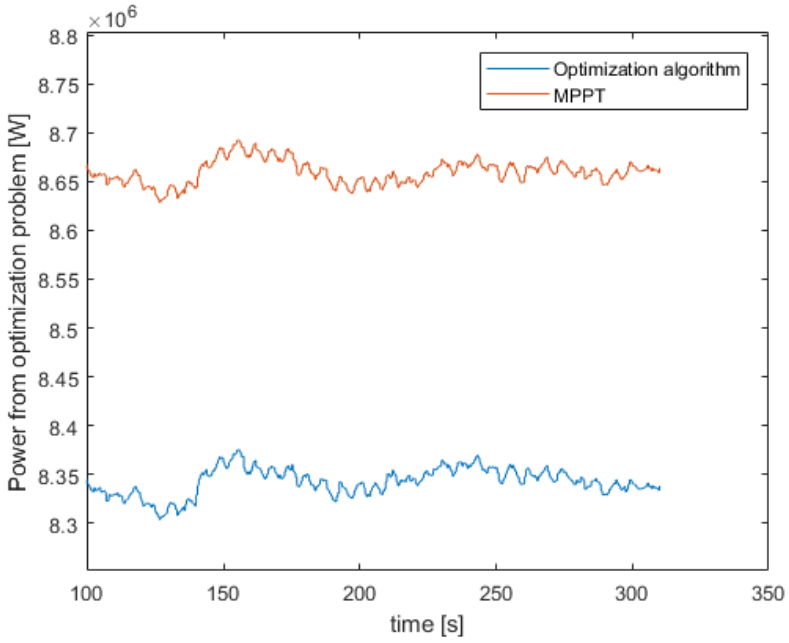

Figure 6.11: Total mechanical power captured by the wind farm

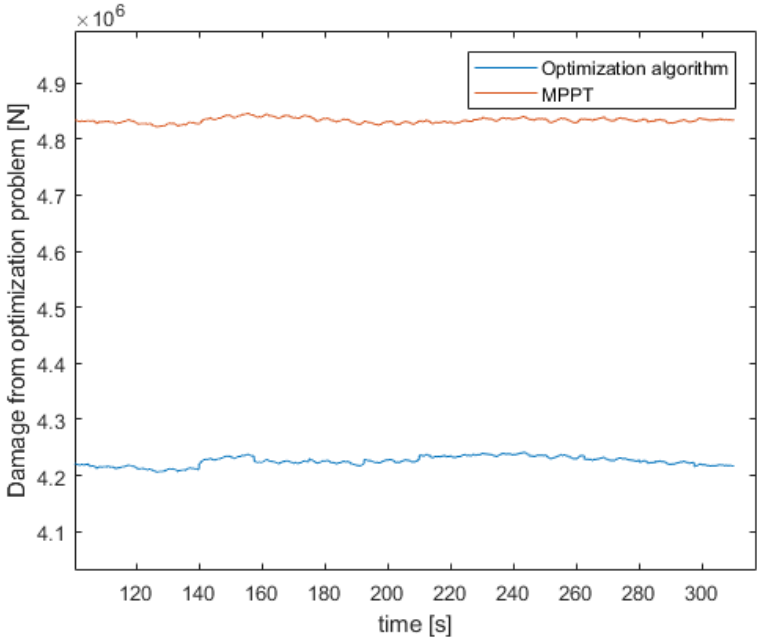

Figure 6.12: Total thrust (loads) acting on the wind farm

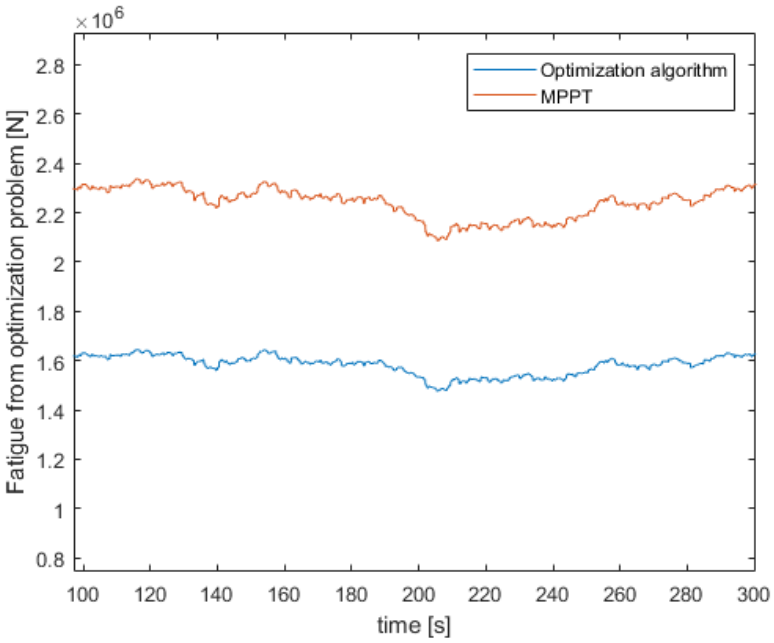

Figure 6.13: Total fatigue damage acting on the wind farm

In Figure 6.14, the output of the reference computation part of the algorithm can be observed. Particular attention can be done on the values, that are always than the maximum given by the Betz limit of 0.33, which is by definition the reference value for the MPPT algorithm (a-MPPT = 0.33 for all the turbines). As can be noticed in Figure 6.14, WT4 has an axial induction factor greater than the other turbines, due to the reduction of wake interactions and a lower input wind speed. So the WT4 can extract more power w.r.t. the others in the analyzed wind farm.

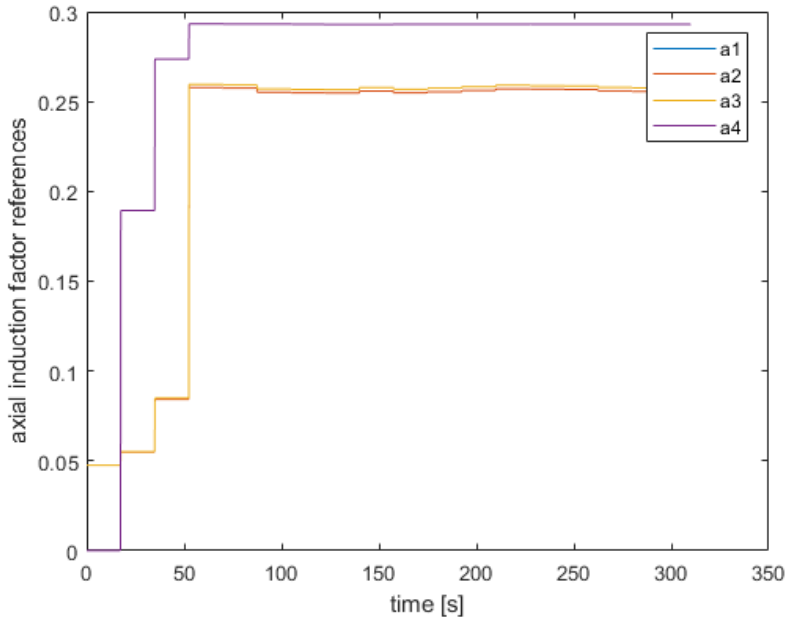

Figure 6.14: Axial induction factor reference values computed from the supervisory control

In Figure 6.15, shows the reference values for the tip speed ratio, that is the output of the second optimization algorithm. The values, that are all around 7 and 8, which are reasonable values.

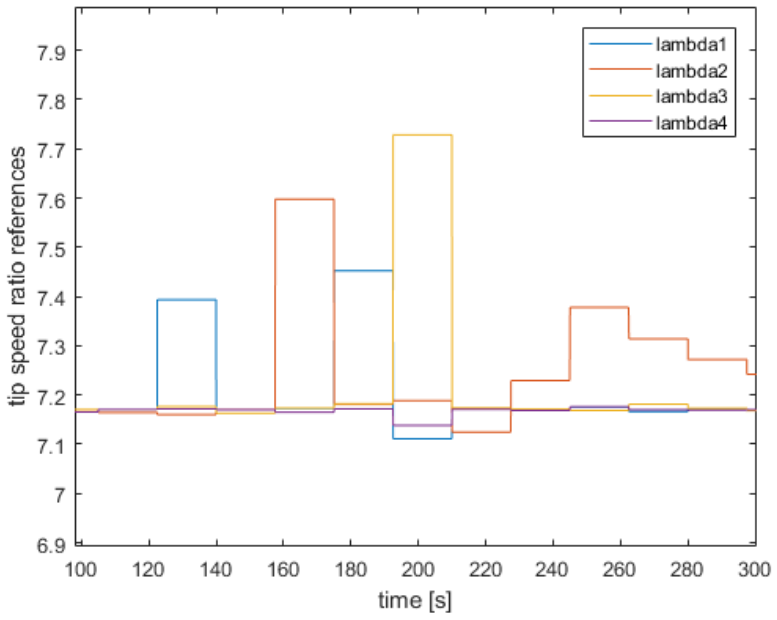

Figure 6.15: Axial induction factor reference values computed from the supervisory control

Chapter 7

CONCLUSIONS AND FUTURE RESEARCH

In this final chapter, a discussion on the results obtained and a general review of possible future research topics is presented.

7.1 Conclusions

In chapter 1, an introduction to the research topic and the relative state of the art has been presented. Moreover, how the various subsystems interacts with each other is described.
In chapter 2, a simple model of an Horizontal Axis Wind Turbine is introduced. However, this model still lacks of the mechanical characteristics such as the inertia of the turbine blades, also the gearbox system could be improved in details, both for losses and for transmission of kinetic energy.
A simple wake model is defined, based on the well known Jensen wake model. This model can describe, in a simple and linear way, the effect of the wake interactions and the consequences on power production of the system. Still, this model lacks of other useful information such as added turbulence at the exit of the turbine and behaviour of the wind in detailed way.
In chapter 3, the model for a doubly fed induction generator, the relative power conversion system and the grid connection system have been presented. The system has been modeled with the help of the Simscape libraries, and in chapter 6 it has been shown how the system measurements correspond to what it should be expected. Nonetheless, the modeling of the power converter has been made with ideal switches, which neglect the losses and delays in the power conversion.
In chapter 4, the vector control for both the converters has been implemented. The super-twisting sliding mode control, present interesting features of robustness to uncertainties and a good tracking capacity for the speed control loop of the DFIM. However, this kind of control algorithm is not an good solution instead for the grid side converter, in which DC-bus voltage still presents high ripples between the reference value.
In chapter 5, an optimization algorithm for a wind farm is presented, and the results shows how, with reference to the MPPT algorithm, the extracted power is reduced, also the damages and fatigue imposed on the turbines is reduced.This means that the life-span of the turbines could be increased in exchange of minor energy production.
In chapter 6, the results for the previously described chapters and arguments has been presented.

7.2 Future research

Future advancement for this research, could aim to provide a more accurate model description and a better control algorithm for the management of the single turbine and of entire wind farm. More precisely:

1. The major issue in the project has been the development of the wind turbine mechanical model, which lacks of many important design requirements. In particular the definition of a drive train model including the inertias of the system, is fundamental for future developments, considering that the fatigue damage reduction analyzed in chapter 5 could also affect the drive train system.

2. The super-twisting sliding mode control algorithm has showed to be not effective for the grid side converter, other control techniques, such as higher order sliding mode control or other control techniques with a continuous control command could improve the system performances.

3. The Jensen wake model lacks of estimations regarding the turbulence fluxes in output of a wind turbine, lacking in details regarding possible wake meandering effects. The implementation of a more detailed wake model could help to have a better prediction of the input wind in the turbines. Consequently a better understanding of the system, fundamental issue regarding the design of a good supervisory control system.

Appendix

Jensen wake model

Based on the formulas described before, the code inside the function block is the following:

```
function [v1,v2,v3,v4,tau2,tau3,tau4] = Jensen(Uinf)

alfa = 0.005;
r0 = 100;
A0 = pi*r0^2
% position of the wind turbines in the xy plane

pT1 = [200,200];

pT2 = [800,275];

pT3 = [700,100];

pT4 = [1600,230];

plot(pT1(1),pT1(2),'x',pT2(1),pT2(2),'x',pT3(1),pT3(2),'x',pT4(1),pT4(2),'x')

% WIND TURBINE 1
v1 = real(Uinf);

% WIND TURBINE 2
a2 = 0.2;
CT2 = 4*a2*(1-a2);
x12 = abs(pT2(1) - pT1(1));
r12 = r0 + alfa*x12;
d12 = abs(pT2(2) - pT1(2));

if d12 ~= 0

    z12 = real((1/d12)*sqrt(4*(d12^2)*(r12^2)-(d12^2-r0^2+r12^2) ));
    L12 = (d12^2-r0^2+r12^2)/(2*d12);
    Ash12 = (r12^2)*acos(complex(L12/r12))+(r0^2)*acos((complex(d12-L12)/r12))-d12*z12;
```

```
    if Ash12 < 0
       Ash12 = 0;
    end

else

    Ash12 = A0;

end

v2 = real(Uinf*(1 - (1- sqrt(1-CT2))*((r0/r12)^2)*(Ash12/A0)));

tau2 = (2*x12)/(Uinf+v2)

% WIND TURBINE 3
a3 = 0.2;
CT3 = 4*a3*(1-a3);
x13 = abs(pT3(1) - pT1(1));
r13 = r0 + alfa*x13;
d13 = abs(pT3(2) - pT1(2));

if d13 ~= 0

    z13 = real((1/d13)*sqrt(4*(d13^2)*(r13^2)-(d13^2-r0^2+r13^2) ));
    L13 = (d13^2-r0^2+r13^2)/(2*d13);
    Ash13 = (r13^2)*acos(complex(L13/r13))
            +(r0^2)*acos(complex((d13-L13)/r13)) -d13*z13;
    if Ash13 < 0
       Ash13 = 0;
    end

else

    Ash13 = A0;

end

v3 = real(Uinf*(1- (1-sqrt(1-CT3))*((r0/r13)^2)*(Ash13/A0)));
tau3 = (2*x13)/(Uinf+v3)

% WIND TURBINE 4
a4 = 0.2;
CT4 = 4*a4*(1-a4);

x14 = abs(pT4(1) - pT1(1));
r14 = r0 + alfa*x14
d14 = abs(pT1(2) - pT4(2));
```

```
if d14 ~= 0

    z14 = (1/d14)*sqrt(4*(d14^2)*(r14^2)-(d14^2-r0^2+r14^2) )
    L14 = (d14^2-r0^2+r14^2)/(2*d14);
    Ash14 = (r14^2)*acos(complex(L14/r14))
            +(r0^2)*acos(complex((d14-L14)/r14)) -d14*z14;
    if Ash14 < 0
       Ash14 = 0;
    end

else

    Ash14 = A0;

end



x24 = abs(pT4(1) - pT2(1));
r24 = r0 + alfa*x24
d24 = abs(pT2(2) - pT4(2));

if d24 ~= 0

    z24 = (1/d24)*sqrt(4*(d24^2)*(r24^2)-(d24^2-r0^2+r24^2) )
    L24 = (d24^2-r0^2+r24^2)/(2*d24);
    Ash24 = (r24^2)*acos(complex(L24/r24))
            +(r0^2)*acos(complex((d24-L24)/r24)) -d24*z24;
    if Ash24 < 0
       Ash24 = 0;
    end

else

    Ash24 = A0;

end



x34 = abs(pT4(1) - pT3(1));
r34 = r0 + alfa*x34;
d34 = abs(pT3(2) - pT4(2));

if d34 ~= 0

    z34 = (1/d34)*sqrt(4*(d34^2)*(r34^2)-(d34^2-r0^2+r34^2) );
    L34 = (d34^2-r0^2+r34^2)/(2*d34);
```

```
    Ash34 = (r34^2)*acos(complex(L34/r34))
            +(r0^2)*acos(complex((d34-L34)/r34)) -d34*z34;
    if Ash34 < 0
       Ash34 = 0;
    end

else

    Ash34 = A0;

end



v4 = real(Uinf*(1-( ((1-sqrt(1-CT4))*((r0/r14)^2)*(Ash14/A0))
            +((1-sqrt(1-CT4))*((r0/r24)^2)*(Ash24/A0))
            +((1-sqrt(1-CT4))*((r0/r34)^2)*(Ash34/A0)))));

tau4 = (2*x14)/(Uinf+v4)
```

Bibliography

[1] L. Y. Pao and K. E. Johnson. *A tutorial on the dynamics and control of wind turbines and wind farms*, 2009 American Control Conference, St. Louis, MO, 2009, pp. 2076-2089.

[2] S. Boersma et al.. *A tutorial on control-oriented modeling and control of wind farms*, 2017 American Control Conference (ACC), Seattle, WA, 2017, pp. 1-18.

[3] E. Capello, T. Wada, E. Punta and Y. Fujisaki. *Minimax Optimization of Fatigue Loads in a Wind Farm and its Realization Via Sliding Mode Controller of Wind Turbines*, 2018 IEEE Conference on Control Technology and Applications (CCTA), Copenhagen, 2018, pp. 430-435.

[4] Gonzalez-Longatt, Francisco Wall, Peter Terzija, V. *Wake effect in Wind Farm Performance: Steady-State and Dynamic Behaviour*, (2012) Renewable Energy. 39. 329–338

[5] Hwang, Chulsang Jeon, Jin-Hong Kim, Gyeong-Hun Kim, Eungsang Park, Minwon Yu, In-Keun. *Modelling and simulation of the wake effect in a wind farm*, (2015) Journal of International Council on Electrical Engineering. 5. 74-77.

[6] Jensen, N.O. *A note on wind generator interaction*, 1983. 16 p. (Risø-M; No. 2411)

[7] M. J. Churchfield *Review of Wind Turbine Wake Models and Future Directions (Presentation)*, NREL (National Renewable Energy Laboratory). NREL/PR-5000-60208. https://www.nrel.gov/docs/fy14osti/60208.pdf.

[8] Yu Zou *Induction Generator in Wind Power Systems*, Induction Motors - Applications, Control and Fault Diagnostics, Raul Igmar Gregor Recalde, IntechOpen, DOI: 10.5772/60958. Available from: https://www.intechopen.com/books/induction-motors-applications-control-and-fault-diagnostics/induction-generator-in-wind-power-systems

[9] Emrah Kulunk. *Aerodynamics of Wind Turbines*, Fundamental and Advanced Topics in Wind Power, Rupp Carriveau, IntechOpen, DOI: 10.5772/17854. Available from: https://www.intechopen.com/books/fundamental-and-advanced-topics-in-wind-power/aerodynamics-of-wind-turbines

[10] Magdi Ragheb and Adam M. Ragheb. *Wind Turbines Theory - The Betz Equation and Optimal Rotor Tip Speed Ratio*, Fundamental and Advanced Topics in Wind Power, Rupp Carriveau, IntechOpen, DOI: 10.5772/21398. Available from: https://www.intechopen.com/books/fundamental-and-advanced-topics-in-wind-power/wind-turbines-theory-the-betz-equation-and-optimal-rotor-tip-speed-ratio

[11] J. K. Sethi, D. Deb and M. Malakar. *Modeling of a wind turbine farm in presence of wake interactions*, 2011 International Conference on Energy, Automation and Signal, Bhubaneswar, Odisha, 2011, pp. 1-6.

[12] K. E. Johnson and N. Thomas. *Wind farm control: Addressing the aerodynamic interaction among wind turbines*, 2009 American Control Conference, St. Louis, MO, 2009, pp. 2104-2109.

[13] F. Spertino. *Wind power systems (short handbook)*, dec 2016, Politecnico di Torino

[14] Abad, Gonzalo Iwanski, Grzegorz. *Properties and Control of a Doubly Fed Induction Machine*, Power Electronics for Renewable Energy Systems, Transportation and Industrial Applications. 270-318.

[15] John Fletcher and Jin Yang. *Introduction to the Doubly-Fed Induction Generator for Wind Power Applications*, Paths to Sustainable Energy, Jatin Nathwani and Artie Ng, IntechOpen, DOI: 10.5772/12889. Available from: https://www.intechopen.com/books/paths-to-sustainable-energy/introduction-to-the-doubly-fed-induction-generator-for-wind-power-applications

[16] Muller, S Deicke, M De Doncker, Rik. *Doubly fed induction generator systems for wind turbines*, Industry Applications Magazine, IEEE. 8. 26 - 33.

[17] Jasinski, Marek Stynski, Sebastian Mlodzikowski, Pawel Malinowski, Mariusz. *AC-DC-AC Converters for Distributed Power Generation Systems.*, Power Electronics for Renewable Energy Systems, Transportation and Industrial Applications. 319-364

[18] Gonzalo Abad; Jesús López; Miguel Rodríguez; Luis Marroyo; Grzegorz Iwanski *Back-to-Back Power Electronic Converter*, Doubly Fed Induction Machine: Modeling and Control for Wind Energy Generation Applications , IEEE, 2011, pp.100-167.

[19] Wenping Cao, Ying Xie and Zheng Tan. *Wind Turbine Generator Technologies*, Advances in Wind Power, Rupp Carriveau, IntechOpen, DOI: 10.5772/51780. Available from https://www.intechopen.com/books/advances-in-wind-power/wind-turbine-generator-technologies

[20] A. Cavagnino. *Appunti delle lezioni*, Macchine elettriche II, parte di Dinamica delle Macchine elettriche, Politecnico di Torino

[21] C. Novara. *Nonlinear control and aerospace applications lecture notes*, Politecnico di Torino

[22] A. Levant. *Introduction to high-order sliding modes*, School of Mathematical Sciences, Tel-Aviv University, Israel, 2002-2003

[23] DeCarlo, Raymond A. and Stanislaw H. Zak. *A quick introduction to sliding mode control and its applications 1.*, 2008, Università degli studi di Cagliari, dipartimento di ingegneria elettrica ed elettronica

[24] Beltran, B Benbouzid, Mohamed Ahmed-Ali, Tarek. *econd-Order Sliding Mode Control of a Doubly Fed Induction Generator Driven Wind Turbine*, IEEE Transactions on Energy Conversion - IEEE TRANS ENERGY CONVERS. 27. 261-269.

[25] J. J. Barradas-Berglind and R. Wisniewski. *Wind farm axial-induction factor optimization for power maximization and load alleviation*, 2016 European Control Conference (ECC), Aalborg, 2016, pp. 891-896.

[26] Mathworks Inc. *Constrained Nonlinear Optimization Algorithms MATLAB*, https://www.mathworks.com/help/optim/ug/constrained-nonlinear-optimization-algorithms.html

[27] Waltz, R., Morales, J., Nocedal, J. et al. *An interior algorithm for nonlinear optimization that combines line search and trust region steps*, Math. Program. (2006) 107: 391. https://doi.org/10.1007/s10107-004-0560-5

[28] R. Fadaeinedjad, M. Moallem and G. Moschopoulos *Simulation of a Wind Turbine With Doubly Fed Induction Generator by FAST and Simulink*, in IEEE Transactions on Energy Conversion, vol. 23, no. 2, pp. 690-700, June 2008.

[29] Göçmen, Tuhfe van der Laan, M. Paul Réthoré, Pierre-Elouan Peña Diaz, Alfredo Chr. Larsen, Gunner Ott, Søren *Wind turbine wake models developed at the technical university of Denmark: A review*, Renewable and Sustainable Energy Reviews. 60. 752-769. 10.1016/j.rser.2016.01.113.

[30] L. Djilali, E. N. Sanchez and M. Belkheiri *Neural sliding mode field oriented control for DFIG based wind turbine*, 2017 IEEE International Conference on Systems, Man, and Cybernetics (SMC), Banff, AB, 2017, pp. 2087-2092.

[31] O. Barambones and J. M. Gonzalez de Durana *Wind turbine control scheme based on adaptive sliding mode controller and observer*, 2015 IEEE 20th Conference on Emerging Technologies Factory Automation (ETFA), Luxembourg, 2015, pp. 1-7.

[32] Corradini, Maria Letizia Ippoliti, Gianluca Orlando, Giuseppe *Robust Control of Variable-Speed Wind Turbines Based on an Aerodynamic Torque Observer*, IEEE Transactions on Control Systems Technology. 21. 1199-1206. 10.1109/TCST.2013.2257777.

[33] Y. Mishra, S. Mishra, M. Tripathy, N. Senroy and Z. Y. Dong *Improving Stability of a DFIG-Based Wind Power System With Tuned Damping Controller*, in IEEE Transactions on Energy Conversion, vol. 24, no. 3, pp. 650-660, Sept. 2009.

[34] Poitiers, Frederic Bouaouiche, T Machmoum, Mohamed *Advanced control of a doubly-fed induction generator for wind energy conversion*, Electric Power Systems Research. 79. 1085-1096. 10.1016/j.epsr.2009.01.007. (2009)

[35] Merida, Jovan Davila, Jorge Aguilar, Luis. *Robust quasi-continuous sliding-mode control of a variable-speed wind turbine*, CCE 2012 - 2012 9th International Conference on Electrical Engineering, Computing Science and Automatic Control. 1-6. 10.1109/ICEEE.2012.6421196.

[36] Beltran, B Ahmed-Ali, Tarek Benbouzid, Mohamed. *Sliding Mode Power Control of Variable Speed Wind Energy Conversion Systems*, Proceedings of IEEE International Electric Machines and Drives Conference, IEMDC 2007. 2. 943 - 948. 10.1109/IEMDC.2007.382801.

[37] Merida, Jovan Aguilar, Luis Davila, Jorge. *Analysis and synthesis of sliding mode control for large scale variable speed wind turbine for power optimization*, Renewable Energy. 71. 715-728. 10.1016/j.renene.2014.06.030. (2014)

[38] Evangelista, Carolina Puleston, P Valenciaga, F Fridman, Leonid. . *Lyapunov Designed Super-Twisting Sliding Mode Control for Wind Energy Conversion Optimization*, IEEE Transactions on Industrial Electronics. 60. 538 - 545. 10.1109/TIE.2012.2188256. (2013)

[39] Spudic, Vedrana. *Hierarchical wind farm control for power/load optimization.*, (2019)

[40] F. Heer, P. M. Esfahani, M. Kamgarpour and J. Lygeros. *Model based power optimisation of wind farms*, 2014 European Control Conference (ECC), Strasbourg, 2014, pp. 1145-1150.

[41] Spudic, Vedrana Jelavić, Mate Baotic, Mato. *Wind Turbine Power References in Coordinated Control of Wind Farms*, Automatika. 52. 82-94. 10.1080/00051144.2011.11828408.

[42] Abdullah, Majid Yatim, Abdul Halim Tan, Chee Wei Rahman, Saidur. *Review of maximum power point tracking algorithms for wind energy systems*, Renewable and Sustainable Energy Reviews. 16. 3220-3227. 10.1016/j.rser.2012.02.016. (2012)

[43] Musunuri, Shravana L. Ginn III, H. *Comprehensive review of wind energy maximum power extraction algorithms*, Power and Energy Society General Meeting. 1-8. 10.1109/PES.2011.6039023. (2011)

[44] González, Javier Burgos Payán, Manuel Santos, Jesús Gonzalez, Angel. *Maximizing the overall production of wind farms by setting the individual operating point of wind turbines*, Renewable Energy. 80. 10.1016/j.renene.2015.02.009. (2015)

[45] Zhang, Jinhua Yongqian, Liu Tian, De Yan, Jie. *Optimal power dispatch in wind farm based on reduced blade damage and generator losses*, Renewable and Sustainable Energy Reviews. 44. 10.1016/j.rser.2014.12.008. (2015)